PHYSICAL REVIEW B VOLUME 50, NUMBER 9 1 SEPTEMBER 1994-I

Angular dependence of ferromaguetic resonance in exchange-coupled Co/Ru/Co trilayer structures

Z. Zhang, L. Zhou, and P. E. Wigen
Department of Physics, The Ohio State University, Columbus, Ohio 43210

K. Ounadjela
Institut de Physique et Chimie des Matériaux de Strasbourg, Groupe d'Etudes des Materiaux Metalliques, 67070 Strasbourg, France
(Received 30 March 1994)

The angular dependence of the dispersion relation is calculated for a system consisting of two ferromagnetic layers exchange coupled through a nonmagnetic spacer layer. Special attention has been focused on the resonance behavior in the unsaturated state of an antiparallel coupled system. The variation of both the acoustic mode and the optic mode with the external-field orientation is significantly modified from that in a noncoupled system and can be used to accurately evaluate the interlayer exchange-coupling strength $A(\theta_{12})$ as a function of the angle between the magnetization vectors in the two magnetic layers. Based on the exchange-coupled resonance theory, the angular dependence of ferromagnetic resonance (FMR) measurements has been performed on several series of symmetrical and asymmetrical Co/Ru/Co structures at X-band and K-band frequencies with the temperature ranging from 10 to 300 K. Only the bilinear exchange-coupling coefficient A_{12} was observed in these systems. The biquadratic contribution is more than two orders of magnitude smaller than A_{12}. For the symmetrical Co(32 Å)/Ru(t_{Ru})/Co(32 Å) series, oscillatory interlayer exchange coupling was observed as a function of the Ru thickness t_{Ru}. The oscillation period ($\sim$12 Å) and phase do not vary with temperature. However, the oscillation amplitude is significantly enhanced at low temperatures, following roughly the relationship $A_{12} \propto (T/T_0)/\sinh(T/T_0)$ predicted by the theoretical models. For the asymmetrical Co(32 Å)/Ru(t_{Ru})/Co(t_2) structures, variation of the exchange coupling strength as a function of t_2 has also been observed for several series within which t_{Ru} is constant. The variation length Δt_2 between maximum and minimum coupling strength is rather large (about 10 Å) and consistent from series to series.

I. INTRODUCTION

The interlayer exchange coupling between ferromagnetic layers mediated by nonmagnetic spacers is believed to be one of the key factors for many properties observed in magnetic/nonmagnetic artificial structures. One example is the giant magnetoresistance which is related to antiparallel ordering between adjacent ferromagnetic layers.[1,2] Currently two experimental methods have been widely used to investigate the exchange-coupling strength based on spin-wave resonance theory. One is ferromagnetic resonance (FMR) and the other is Brillouin light scattering (BLS).

The spin-wave dispersion relation for trilayer structures[3,4] and multilayer structures[5] has been derived by several groups. In their models, the external field is assumed to be in the film plane and large enough that the magnetic moment in each layer is along the field direction. Usually these experimental conditions can be readily achieved since the interlayer exchange coupling field is very small ($\leq$1 kG) in most of the structures. However, in some of the Fe/Cr, Co/Ru structures, the ferromagnetic layers are strongly antiparallel coupled with the coupling field on the order of several kG. As result, some samples are not saturated under the resonance conditions.[6–8] Wigen *et al.*[9] and Cochran *et al.*[8] independently calculated the dispersion relations in this situation and found that the resonance spectra are significantly modified from the previous predictions in which the magnetic moment is assumed to be saturated.

The derivation assumed that the external field is applied either in the film plane[2–5,8,9] or perpendicular to the film plane.[9] However, in some cases, the experimental results from just the parallel and perpendicular resonance spectra will not provide enough information to allow an accurate evaluation of the exchange coupling strength. This is due to the fact that the dispersion relation in an exchange-coupled multilayer system depends not only on the interlayer exchange coupling strength but also on the internal anisotropy energies and the g value within each ferromagnetic layer. On the other hand, FMR data with the external field rotated continuously from the parallel to the perpendicular orientation with respect to the film plane can provide significant supplementary information. For this purpose, the angular dependence of the FMR spectra for a trilayer structure will be calculated in Sec. II. Experimentally Co/Ru/Co trilayer structures were chosen for the FMR measurements. Because of the large variation in the exchange coupling in Co/Ru structures,[7,10] the experimental results at X-band and K-band frequencies provide a good test of the theoretical predictions for both the saturated and the unsaturated configurations. In Sec. III, FMR data for several series of Co/Ru/Co trilayer structures are provided. From these data, the interlayer exchange coupling strength as well as the internal anisotropy ener-

0163-1829/94/50(9)/6094(19)/$06.00

gy were evaluated and the results will be reported in Sec. IV.

II. FERROMAGNETIC DISPERSION RELATION

The exchange-coupled system to be discussed in this paper consists of two ferromagnetic layers separated by a nonmagnetic spacer as shown in Fig. 1. The calculation of the dispersion relation for this system can be simplified from the spin-wave theory of a single ferromagnetic film based on the following considerations. First, since the microwave pumping field is uniformly applied across the film plane in the FMR experiment, the spin-wave modes with in-plane wave vector $k_{\parallel}\neq 0$ are not excited, i.e., no spatial variation along the directions parallel to the film plane is assumed. Second, only the lowest-order spin-wave mode across each ferromagnetic layer will be considered. Any higher-order spin-wave modes would need much larger external field ($>10^3$ kOe) to be excited as the thickness of each ferromagnetic layer is on the order of a few nm. Third, in the very thin-film limit for which the thickness is less than the magnetic correlation length (domain-wall thickness), there is no real "surface region" within each layer. Any surface-interface pinning condition may be represented by introducing an effective anisotropy field averaged across the layer having a strength which varies inversely with the layer thickness.[11] Fourth, exchange coupling is the only interlayer coupling term to be considered. The dipole-dipole interaction between the spin waves in the two magnetic layers disappears because the in-plane wave vector $k_{\parallel}=0$.[12] Finally, the exchange coupling between the two magnetic layers is equivalent to having an extra torque on the surface spins of each magnetic layer which can be replaced by an exchange field averaged across the layer.[13] Based on these considerations, the lowest-order spin-wave mode within each layer is close to the uniform precession mode. Thus, a single magnetization vector $\mathbf{M}_1$ (or $\mathbf{M}_2$) will be used to represent the behavior of the magnetic moment in the first (or second) ferromagnetic layer.

It is further assumed that the two ferromagnetic layers are made of the same material, having the same saturation magnetization $|\mathbf{M}_1|=|\mathbf{M}_2|=M_S$ and same g value. The energies involved in this exchange-coupled system are the following.

(1) Zeeman energy,

$$\sum_i -(t_i \mathbf{H}_0\cdot\mathbf{M}_i) ,$$

where $\mathbf{H}_0$ is the external field and $i=1$ (or 2) refers to the first (or the second) ferromagnetic layer having the thickness of t_1 (or t_2).

(2) Effective anisotropy energies,

$$\sum_i t_i \left[\frac{1}{2} H_{u2,i}^{\text{eff}} \frac{M_{i,\parallel}^2}{M_s} + \frac{1}{4} H_{u4,i} \frac{M_{i,\parallel}^4}{M^3} \right] ,$$

where the z axis is normal to the film plane and $M_{i,\parallel}$ is the in-plane component of the magnetization of the ith layer. $H_{u2,i}^{\text{eff}}$ includes the demagnetization field $-4\pi M_s$ and the perpendicular anisotropy field $2K_{u2,i}/M_s$ which corresponds to a contribution of the magnetocrystalline anisotropy field of an hcp structure with its c axis normal to the film plane ($2K_{mc}/M_s$), and to the surface anisotropy field ($4K_s/t_i M_s$). $H_{u4,i}=4K_{u4,i}/M_s$ is the higher-order anisotropy term proportional to $M_{i,\parallel}^4$. In general, the perpendicular anisotropy fields $H_{u2,i}^{\text{eff}}$ and $H_{u4,i}$ may differ from one layer to the other due to the differences in film thicknesses or surface pinning conditions. The in-plane anisotropy energy is not included in the calculation because of its very small value (about 2 orders of magnitude smaller than $H_{u2,i}^{\text{eff}}$ due to the sixfold symmetry in the film plane of the hcp Co/Ru/Co trilayer structures).

(3) Interlayer exchange energy,

$$A_{12}\frac{\mathbf{M}_1\cdot\mathbf{M}_2}{M_1 M_2} ,$$

where A_{12} is the bilinear exchange energy constant per unit surface area. The sign of A_{12} is chosen so that it is positive for an antiparallel coupled system and negative for a parallel coupled system. Recently a higher-order biquadratic exchange term which is proportional to $(\mathbf{M}_1\cdot\mathbf{M}_2/M_1M_2)^2$ was observed in some fcc multilayer structures.[14,15] However, as will be shown in a later section, the biquadratic term in the hcp Co/Ru/Co trilayer structures is more than 2 orders of magnitude smaller than the bilinear term, and therefore, it is neglected in these calculations.

Using the polar coordinate system shown in Fig. 1, the energy per unit surface area can be written as

$$\begin{aligned}\mathcal{E}=\sum_{i=1}^{2} t_i[&-M_s H_0(\cos\theta_H\cos\theta_i+\sin\theta_H\sin\theta_i\cos\phi_i)\\&+\tfrac{1}{2}H_{u2,i}^{\text{eff}}M_s\sin^2\theta_i+\tfrac{1}{4}H_{u4,i}M_s\sin^4\theta_i]\\&+A_{12}[\cos\theta_1\cos\theta_2+\sin\theta_1\sin\theta_2\cos(\phi_1-\phi_2)] .\end{aligned} \tag{1}$$

Here θ_i is the polar angle of the magnetization direction $\mathbf{M}_i$ to the z axis which is normal to the film plane and ϕ_i is the azimuth angle to the x axis in the film plane. The external field $\mathbf{H}_0$ is assumed to be in the $x-z$ plane with an angle of θ_H from the z axis.

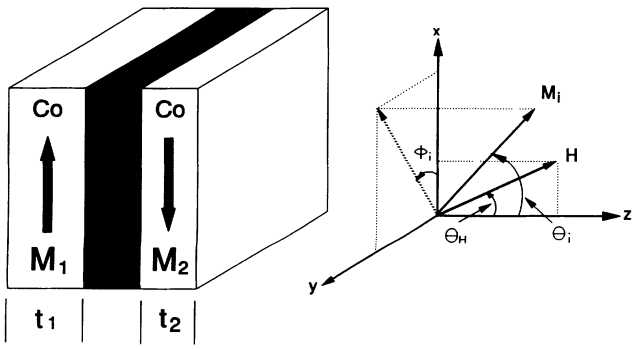

FIG. 1. The trilayer structure and coordinate system used in the model.

A. Equilibrium positions and *M-H* loops

The system is assumed to have an easy-plane anisotropy field, i.e., $H_{u2,i}^{\text{eff}}+H_{u4,i}<0$, where $i=1$ and 2. The equilibrium positions of the magnetization vectors can be obtained by minimizing the total energy $\mathcal{E}$ with respect to θ_i and ϕ_i.

For an antiparallel exchange-coupled system ($A_{12}>0$), the variation of $\mathbf{M}_1$ and $\mathbf{M}_2$ with the external field, $\mathbf{H}$, depends on the applied field direction θ_H. Assuming $t_1 \geq t_2$ and $|H_{\text{eff},1}| \geq |H_{\text{eff},2}|$, two critical angles $\theta_{\text{cri},1}$ and $\theta_{\text{cri},2}$ exist. In the range $0 \leq \theta_H < \theta_{\text{cri},1}$, $\mathbf{M}_1$ and $\mathbf{M}_2$ will always stay in the $x-z$ plane. With increasing external field, $\mathbf{M}_1$ will rotate from $+x$ axis towards the external field orientation while $\mathbf{M}_2$ starts from the $-x$ axis, passing through the z axis (if $\theta_H \neq 0$) to approach θ_H. There is a sudden change of ϕ_2 from $-180°$ to $0°$ when $\mathbf{M}_2$ is parallel to the z axis as shown in Fig. 2(a).

In the range $\theta_{\text{cri},1} \leq \theta_H < \theta_{\text{cri},2}$, three different processes exist which are characterized by the values of ϕ_1 and ϕ_2. (i) For small field, $\mathbf{M}_1$ and $\mathbf{M}_2$ stay in the $x-z$ plane parallel to the x and $-x$ axis, respectively, and rotate toward the z axis with $\phi_1=0°$ and $\phi_2=-180°$. (ii) When the external field is raised above a critical value, $H_{\text{cr},1}(\theta_H)$, $\mathbf{M}_2$ starts to rotate out of the $x-z$ plane. At the same time, $\mathbf{M}_1$ is expelled out of the $x-z$ plane due to the antiparallel exchange coupling. ϕ_1 and ϕ_2 in this region follow the relationship

$$t_1 \sin\theta_1 \sin\phi_1 = -t_2 \sin\theta_2 \sin\phi_2 \ . \tag{2}$$

(iii) If the external field is further increased above another critical value $H_{\text{cri},2}(\theta_H)$, both $\mathbf{M}_1$ and $\mathbf{M}_2$ are forced back to move within the $x-z$ plane. However, instead of falling into the positive half of the $x-z$ plane (i.e., $\phi=0$), $\mathbf{M}_2$ is in the negative half of the plane ($\phi_2=-180°$) at $H_{\text{cri},2}(\theta_H)$ and remains in this plane but rotates through the z axis toward the applied field orientation with increasing applied field. These three processes are illustrated in Fig. 2(b).

In the range $\theta_H \geq \theta_{\text{cri},2}$, there also exist three regions separated by $H_{\text{cr},1}(\theta_H)$ and $H_{\text{cr},2}(\theta_H)$. The only difference between $\theta_{\text{cr},1} \leq \theta_H \leq \theta_{\text{cri},2}$ and $\theta_H \geq \theta_{\text{cri},2}$ is that in the later case, $\mathbf{M}_2$ will fall into the positive half of the $x-z$ plane (i.e., $\phi_2=0°$) at $H_{\text{cr},2}(\theta_H)$. Therefore, as shown in Fig. 2(c), there is no sudden change of ϕ_2 from $-180°$ to $0°$.

A special case in this range occurs when the external field is applied in the film plane along the x axis ($\theta_H=90°$) as shown in Fig. 2(d). The induced magnetization is constant for

$$H \leq H_{\text{cri},1} = \frac{A_{12}}{t_2 M_s} - \frac{A_{12}}{t_1 M_s}$$

as $\mathbf{M}_1$ and $\mathbf{M}_2$ remain parallel and antiparallel to the x axis, respectively. $\mathbf{M}_1$ and $\mathbf{M}_2$ rotate within the film plane for

$$H_{\text{cri},1} \leq H \leq H_{\text{cri},2} = \frac{A_{12}}{t_2 M_s} + \frac{A_{12}}{t_1 M_s} \ .$$

When the external field is above $H_{\text{cri},2}$, the film is saturated as both $\mathbf{M}_1$ and $\mathbf{M}_2$ are forced to align parallel to the x axis.

Due to the complex form of $\mathcal{E}$ in Eq. (1), it is difficult to get explicit expressions of the critical angles $\theta_{\text{cri},1}$ and $\theta_{\text{cri},2}$. Each one has to be obtained by solving a set of equations simultaneously.

For $\theta_{\text{cri},1}$,

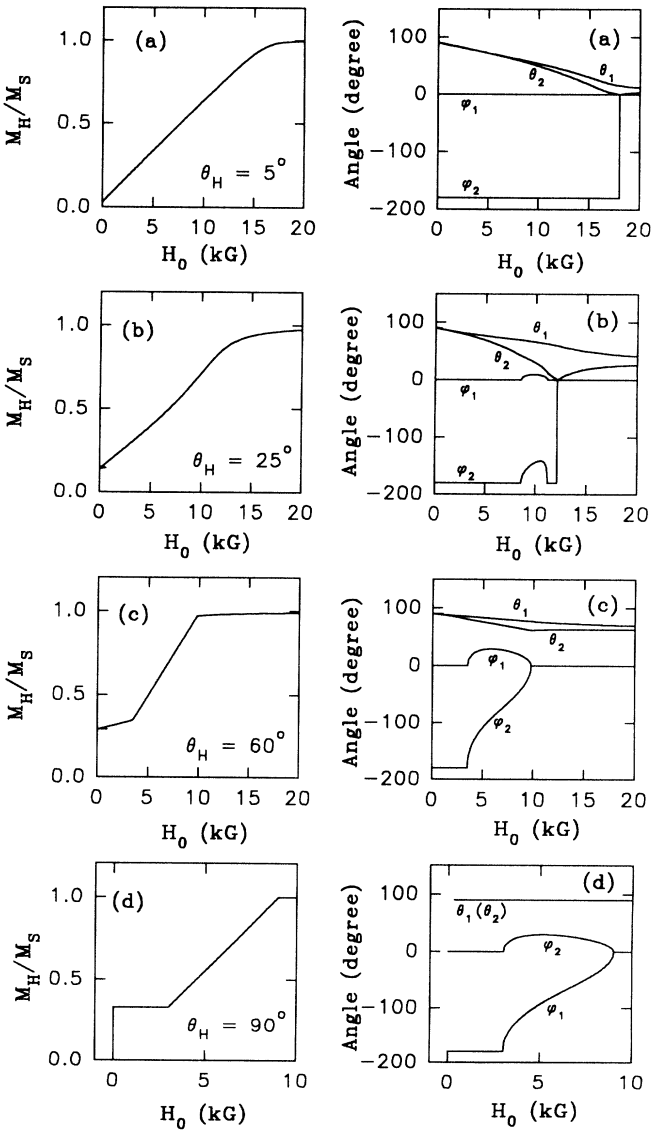

FIG. 2. In-plane hysteresis loop (left) and equilibrium angles of the magnetization vector in each layer (right) for an asymmetrical trilayer system with the external magnetic field applied at (a) 5°, (b) 25°, (c) 60°, and (d) 90° off the perpendicular orientation. The parameters are $t_1/t_2=2$, $H_{2u,1}^{\text{eff}}=-9.5$ kG, $H_{2u,2}^{\text{eff}}=-4.5$ kG, and $A_{12}/t_1M_s=3$ kG which correspond to $\theta_{\text{cri},1}=23.9°$ and $\theta_{\text{cri},2}=28°$ as defined in the text.

$$(H_{u2,1}^{\text{eff}}+H_{u4,1}\sin^2\theta_1)\cos\theta_1=(H_{u2,2}^{\text{eff}}+H_{u4,2}\sin^2\theta_2)\cos\theta_1 ,$$

$$\frac{A_{12}}{t_2M_s}\sin(\theta_1-\theta_{cri,1})-\frac{A_{12}}{t_1M_s}\sin(\theta_2+\theta_{cri,1})$$
$$+(H_{u2,1}^{\text{eff}}+H_{u4,1}\sin^2\theta_1)\cos\theta_1\sin\theta_{cri,1}=0 , \quad (3)$$

$$\frac{d}{d\theta_1}\left[\frac{A_{12}}{t_2M_s}\sin(\theta_1-\theta_{cri,1})-\frac{A_{12}}{t_1M_2}\sin(\theta_2+\theta_{cri,1})\right.$$
$$\left.+(H_{u2,1}^{\text{eff}}+H_{u4,1}\sin^2\theta_1)\cos\theta_1\sin\theta_{cri,1}\right]=0 .$$

For $\theta_{cri,2}$,

$$(H_{u2,1}^{\text{eff}}+H_{u4,1}\sin^2\theta_1)\cos\theta_1=H_{u2,2}^{\text{eff}} ,$$
$$\left[\frac{A_{12}}{t_1M_s}+\frac{A_{12}}{t_2M_s}\cos\theta_1-H_{u2,2}^{\text{eff}}\right]\tan\theta_H=\frac{A_{12}}{t_2M_s}\sin\theta_1 . \quad (4)$$

For special cases, the magnetization process can be simplified. If $t_1=t_2$ (i.e., symmetrical structure), $\theta_{cri,1}=0$ and $H_{cri,1}=0$. As a result, both $\mathbf{M}_1$ and $\mathbf{M}_2$ will rotate out of the $x-z$ plane as the external field is increased from zero. Furthermore, if the magnetic anisotropy energies of the two ferromagnetic layers are identical, $\theta_{cri,2}$ will also be zero, suggesting that $\phi_2=0$ at $H_{cri,2}$. In fact, since the two magnetic layers are identical with each other in this case, θ_i and ϕ_i are symmetric about the $x-z$ plane.

In contrast to the antiparallel coupled system, only one process exists in the parallel exchange-coupled system. At zero field, both $\mathbf{M}_1$ and $\mathbf{M}_2$ stay parallel to the x axis. Upon increasing the external field, they will rotate toward the applied field orientation within the $x-z$ plane. Since the static energy expression of Eq. (1) is independent of ϕ_1 and ϕ_2, the equilibrium positions of the magnetization vectors $\mathbf{M}_1$ and $\mathbf{M}_2$ can be handily obtained by minimizing the energy with respect to θ_1 and θ_2.

B. Dispersion relation

When this exchange-coupled system is located in an applied static magnetic field, the magnetic moment in each layer, if perturbed from their equilibrium orientation, will precess around its equilibrium direction which can be expressed by the relation

$$\frac{1}{\gamma}\frac{d\mathbf{M}_i}{dt}=-\frac{1}{t_i}\mathbf{M}_i\times\mathbf{H}_{\text{eff},i}=\frac{1}{t_i}\frac{\mathbf{M}_i}{M_s}\times\nabla_i\mathcal{E} \quad (i=1,2) , \quad (5)$$

where γ is the gyromagnetic ratio and $\nabla,\mathcal{E}$ can be expressed as

$$\nabla_i\mathcal{E}=\partial\mathcal{E}/\partial\theta_i\hat{e}_{\theta_i}+\frac{1}{\sin\theta_i}\partial\mathcal{E}/\partial\phi_i\hat{e}_{\phi_i} \quad (6)$$

in the polar coordinate system where $\hat{e}_{\theta_i}$ and $\hat{e}_{\phi_i}$ are unit vectors along the θ_i and ϕ_i directions. At the equilibrium position, $\mathbf{M}_i$ is independent of time ($d\mathbf{M}_i/dt=0$), and Eq. (5) will give the same equilibrium conditions as discussed in the previous section. Assuming a small deviation of the magnetic moment $\mathbf{M}_i$ from its equilibrium position $M_s\hat{e}_{r_i}$,

$$\mathbf{M}_i=M_s\hat{e}_{r_i}+m_{\theta_i}\hat{e}_{\theta_i}+m_{\phi_i}\hat{e}_{\phi_i} , \quad (7)$$

the equations of motion can be obtained by expanding Eq. (5) and retaining only terms to the first order of m_{θ_i} and m_{ϕ_i}, where $m_{\theta_i}=M_s\delta\theta_i$ and $m_{\phi_i}=M_s\sin\theta_i\delta\phi_i$ are small deviations of the magnetization along the θ_i and ϕ_i directions, respectively. If the time variation follows the $e^{-i\omega t}$ form, where w is the angular frequency, the following expressions are obtained which are similar to the results published in the literature:[16]

$$\begin{bmatrix}
\frac{iw}{\gamma}+\frac{E_{\theta_1\phi_1}}{t_1M_s\sin\theta_1} & \frac{E_{\phi_1\phi_1}}{t_1M_s\sin^2\theta_1} & \frac{E_{\theta_2\phi_1}}{t_1M_s\sin\theta_1} & \frac{E_{\phi_1\phi_2}}{t_1M_s\sin\theta_1\sin\theta_2} \\
-\frac{E_{\theta_1\theta_1}}{t_1M_s} & \frac{iw}{\gamma}-\frac{E_{\theta_1\phi_1}}{t_1M_s\sin\theta_1} & -\frac{E_{\theta_1\theta_2}}{t_1M_s} & -\frac{E_{\theta_1\phi_2}}{t_1M_s\sin\theta_2} \\
\frac{E_{\theta_1\phi_2}}{t_2M_s\sin\theta_2} & \frac{E_{\phi_1\phi_2}}{t_2M_s\sin\theta_1\sin\theta_2} & \frac{iw}{\gamma}+\frac{E_{\theta_2\phi_2}}{t_2M_s\sin\theta_2} & \frac{E_{\phi_2\phi_2}}{t_2M_s\sin^2\theta_2} \\
-\frac{E_{\theta_1\theta_2}}{t_2M_s} & -\frac{E_{\theta_2\phi_1}}{t_2M_s\sin\theta_1} & -\frac{E_{\theta_2\theta_2}}{t_2M_s} & \frac{iw}{\gamma}-\frac{E_{\theta_2\phi_2}}{t_2M_s\sin\theta_2}
\end{bmatrix}
\begin{bmatrix} m_{\theta_1} \\ m_{\phi_1} \\ m_{\theta_2} \\ m_{\phi_2} \end{bmatrix}=0 . \quad (8)$$

Here $E_{\theta_i\theta_j}=\partial^2\mathcal{E}/\partial\theta_i\partial\theta_j$, $E_{\theta_i\phi_j}=\partial^2\mathcal{E}/\partial\theta_i\partial\phi_j$ and $E_{\phi_i\phi_j}=\partial^2\mathcal{E}/\partial\phi_i\partial\phi_j$. Although these equations are derived for a trilayer structure, they can easily be expanded to an exchange-coupled multilayer system.[17]

The roots of the determinant of the 4×4 matrix on the left-hand side of Eq. (8) will give the dispersion relation of the exchange-coupled trilayer system:

$$\left[\frac{\omega}{\gamma}\right]^4-b\left[\frac{\omega}{\gamma}\right]^2+c=0 , \quad (9)$$

where

$$b=\frac{E_{\theta_1\theta_1}E_{\phi_1\phi_1}-E_{\theta_1\phi_1}^2}{t_1^2M_s^2\sin^2\theta_1}+\frac{E_{\theta_2\theta_2}E_{\phi_2\phi_2}-E_{\theta_2\phi_2}^2}{t_2^2M_s^2\sin^2\theta_2}+2\frac{E_{\theta_1\theta_2}E_{\phi_1\phi_2}-E_{\theta_1\phi_2}E_{\theta_2\phi_1}}{t_1t_2M_s^2\sin\theta_1\sin\theta_2},$$

$$\begin{aligned}c=\frac{1}{t_1^2t_2^2M_s^4\sin^2\theta_1\sin^2\theta_2}[&E_{\theta_1\theta_2}^2E_{\phi_1\phi_2}^2+E_{\theta_1\phi_1}^2E_{\theta_2\phi_2}^2+E_{\theta_1\phi_2}^2E_{\theta_2\phi_1}^2-E_{\theta_1\theta_2}^2E_{\phi_1\phi_1}E_{\phi_2\phi_2}\\&-E_{\phi_1\phi_2}^2E_{\theta_1\theta_1}E_{\theta_2\theta_2}-E_{\theta_1\phi_1}^2E_{\theta_2\theta_2}E_{\phi_2\phi_2}-E_{\theta_1\phi_2}^2E_{\theta_2\theta_2}E_{\phi_2\phi_2}-E_{\theta_2\phi_1}^2E_{\theta_1\theta_1}E_{\phi_1\phi_1}\\&+E_{\theta_1\theta_1}E_{\phi_1\phi_1}E_{\theta_2\theta_2}E_{\phi_2\phi_2}+2E_{\theta_1\theta_1}E_{\phi_1\phi_2}E_{\theta_2\phi_2}E_{\theta_2\phi_2}+2E_{\theta_1\phi_1}E_{\theta_1\phi_2}E_{\phi_1\phi_2}E_{\theta_2\theta_2}\\&+2E_{\theta_1\theta_2}E_{\theta_1\phi_2}E_{\phi_1\phi_2}E_{\theta_2\phi_2}+2E_{\theta_1\theta_2}E_{\theta_1\phi_1}E_{\theta_2\phi_1}E_{\phi_2\phi_2}\\&-2E_{\theta_1\phi_1}E_{\theta_2\phi_2}(E_{\theta_1\theta_2}E_{\phi_1\phi_2}+E_{\theta_1\phi_2}E_{\theta_2\phi_1})-2E_{\theta_1\theta_2}E_{\phi_1\phi_2}E_{\theta_1\phi_2}E_{\theta_2\phi_1}].\end{aligned}$$

Two of the four solutions give negative values of ω/γ and do not correspond to any physical resonance modes. As a result, only two resonance frequencies are obtained at any given field.

As an example, the dispersion relation for a symmetrical parallel coupled system ($t_1=t_2$, $H_{u2,1}^{\text{eff}}=H_{u2,2}^{\text{eff}}=H_{u2}^{\text{eff}}$, $H_{u4,1}=H_{u4,2}=0$, and $A_{12}<0$) is shown in Fig. 3. When the external field is in the film plane ($\theta_H=90°$), the dispersion relation for the two modes has a simple form. One mode (the acoustic mode) corresponds to the rf components of the two magnetization vectors resonating in phase, i.e., $m_{\theta_1}/m_{\theta_2}=m_{\phi_1}/m_{\phi_2}=1$. The exchange energy, which is constant during the precession, does not produce any dynamic contribution to the resonance condition. Therefore, the dispersion relation of the acoustic mode is degenerate with that of a single-layer system. The other mode (the optic mode) corresponds to the rf components of the magnetization vectors resonating out of phase. The exchange energy introduces an extra field

$$H_{\text{ex}}=2A_{12}/t_1M_s=2A_{12}/t_2M_s$$

to the dispersion relation of this mode and shifts the resonance field by a value of H_{ex} from that of the acoustic mode at the same frequency. For this system ($H_{\text{ex}}<0$) the optic mode is observed at the higher frequency or lower magnetic field side of the acoustic mode is degenerate with that of the single-layer system as in the parallel coupled system. The optic mode, which is due to the increase in the exchange energy as the magnetization vectors in the two layers deviate from the parallel orientation. When the external field is applied normal to the film plane ($\theta_H=0$) and larger than the saturation field $-H_{u2}^{\text{eff}}$, similar results are obtained: the acoustic mode is degenerate with that of the single-layer system while the optic mode is shifted to the lower field side of the acoustic mode by a value of $|2H_{\text{ex}}|$ at constant frequencies. For $H<-H_{u2}^{\text{eff}}$, the acoustic mode stays at zero frequency as in the single-layer case. The optic mode is lifted to a rather high-energy state due to the exchange interaction.

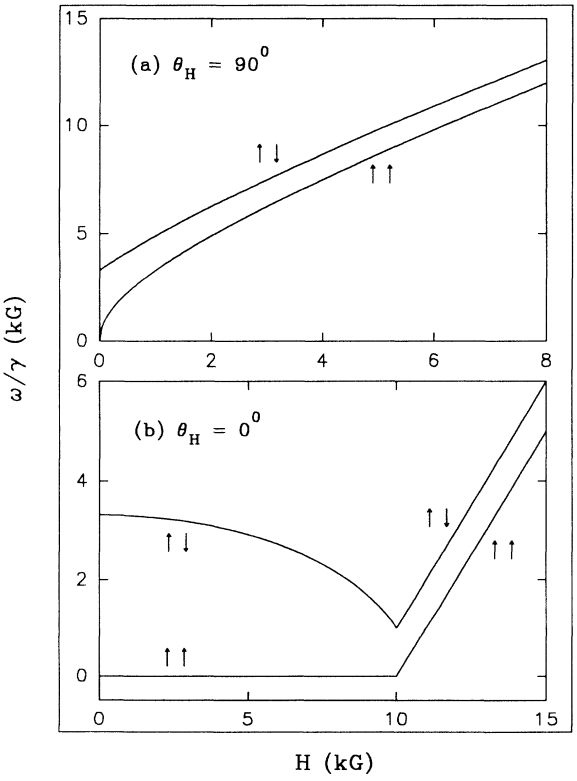

FIG. 3. The dispersion relation for a symmetrical parallel coupled trilayer system with the external field applied (a) parallel and (b) perpendicular to the film plane. The parameters are $H_{u2,1}^{\text{eff}}=H_{u2,2}^{\text{eff}}=-10$ kG and $H_{\text{ex}}=2A_{12}/t_1M_s=2A_{12}/t_2M_s=-1$ kG. ↑↑ (or ↑↓) refers to acoustic mode (optic mode).

When the two ferromagnetic layers in the above-mentioned system are antiparallel coupled, i.e., $A_{12}>0$, the dispersion relation can be quite different as shown in Fig. 4 with the external field applied at different angles. If the external field is larger than the saturation field, the acoustic mode is degenerate with that of the single-layer system as in the parallel coupled system. The optic mode, however, is observed at the lower-frequency or higher-magnetic-field side of the acoustic mode. This shift is due to the decrease in the exchange energy as the magnetization vectors in the two layers deviate from the parallel orientation as opposed to the increase in the exchange energy for the parallel coupled system.

Based on these results, the anisotropy energy can be obtained from the angular-dependent FMR field of the acoustic mode while both the sign and amplitude of A_{12}

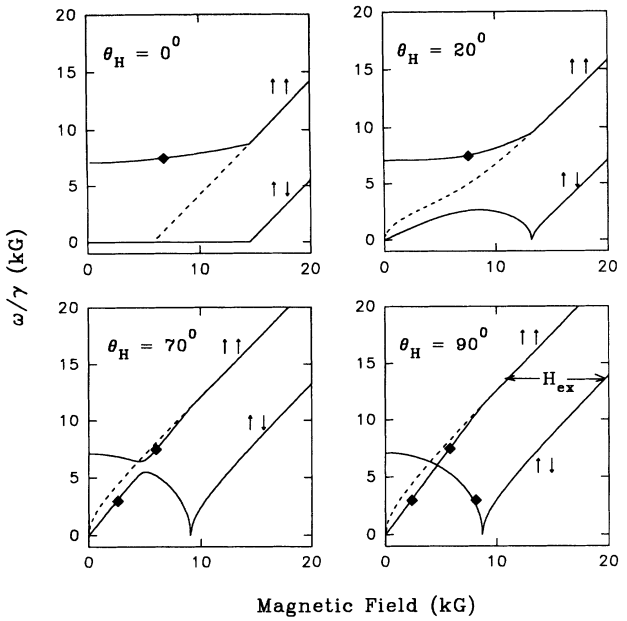

FIG. 4. The dispersion relation for a symmetrical trilayer system with the external field applied at 0°, 20°, 40°, and 90° off the perpendicular orientation. The parameters are $t_1=t_2=32$ Å, $H_{2u,1}^{\text{eff}}=H_{2u,2}^{\text{eff}}=-5.8$ kG, and $H_{\text{ex}}=2A_{12}/t_1M_s=8.7$ kG which are consistent with the observation for the Co(32 Å)/Ru(9 Å)/Co(32 Å) sample. The solid diamonds are experimental FMR data. The dashed lines are the dispersion relation for a single layer (or noncoupled) system, i.e., $A_{12}=0$. ↑↑ (↑↓) refers to acoustic mode (optic mode). As the sample is rotated a gap is shown to develop in the low-field acoustic mode.

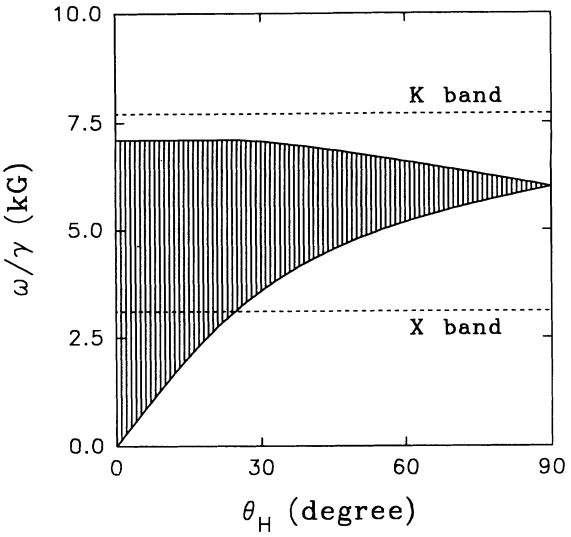

FIG. 5. The frequency gap (shadowed area) as a function of θ_H. The parameters are the same as those used in Fig. 4.

can be evaluated from the field separation between the acoustic mode and the optic mode in the saturated region.

If the symmetrical antiparallel coupled system is unsaturated at resonance, the dispersion relation for both modes is significantly modified from that of a single-layer system as shown by the dashed line in Fig. 4. When the external field is applied in the film plane ($\theta_H=90°$), the resonance frequency of the acoustic mode (↑↑) increases with increasing external field while the frequency of the optic mode (↑↓) decreases. These two modes become degenerate at a particular field value where the two dispersion curves cross each other. When the external field is rotated away from the film plane ($\theta_H<90°$), an energy gap appears near the crossover region as shown in Fig. 4. With decreasing θ_H, the minimum edge of the gap decreases while the maximum edge remains relatively flat. The increase in the width of the gap with decreasing angle is shown in Fig. 5. This unusual behavior indicates that the acousticlike resonance mode will not be observed over a certain θ_H range if the resonance frequency is lower than the maximum of the upper gap edge. On the other hand, the variation of the resonance field with θ_H for these modes can be used to evaluate both A_{12} and the anisotropy energy simultaneously. When the field is applied normal to the film, the optic mode will remain at zero frequency in the unsaturated region while the acoustic mode stays at relatively high frequencies, changing slowly with H_0. If the curve of this acoustic mode moves up or down slightly, due to small changes in A_{12} and/or the internal anisotropy energy, the resonance field corresponding to a fixed frequency value will change significantly. As a result, the FMR spectra at this frequency range can be used to accurately determine the exchange-coupling strength and its variation with the systematic change of the external conditions, such as temperature. An example will be given in the experimental part.

Unlike in the saturation region where the rf component of the magnetization in each layer resonates either in phase or out of phase with each other, there is no simple relation between the dynamic terms of $\mathbf{M}_1$ and $\mathbf{M}_2$ in the unsaturated region except for $\theta_H=0°$ and $\theta_H=90°$. Therefore, the concept of the acoustic mode and the optic mode is no longer appropriate to describe the two resonance modes in the unsaturated region for $0°<\theta_H<90°$.

If the two ferromagnetic layers are not identical, i.e., they might have different uniaxial anisotropy fields and/or different layer thickness, the dispersion relation can be quite different from Fig. 4 due to the complicated magnetization process. In general, the angular dependence of the dispersion relation is shown in Fig. 6. At $\theta_H=0$, one of the resonance modes remains at zero frequency in the unsaturated region while the other mode stays at a relatively high-energy state. As the external field deviates from the perpendicular orientation but satisfies the condition $\theta_H\leq\theta_{\text{cri},1}$, the lower branch in the unsaturated region is lifted above the zero-frequency value and the dispersion relation is continuous in slope. When $\theta_H>\theta_{\text{cri},1}$, two singularities (defined as the point at which the dispersion relation is discontinuous in slope) appear at $H_{\text{cri},1}(\theta_H)$ and $H_{\text{cri},2}(\theta_H)$ which correspond to the magnetization vectors starting to rotate out of and back into the $x-z$ plane, respectively. The lower mode at these singularities has zero resonance frequency. For

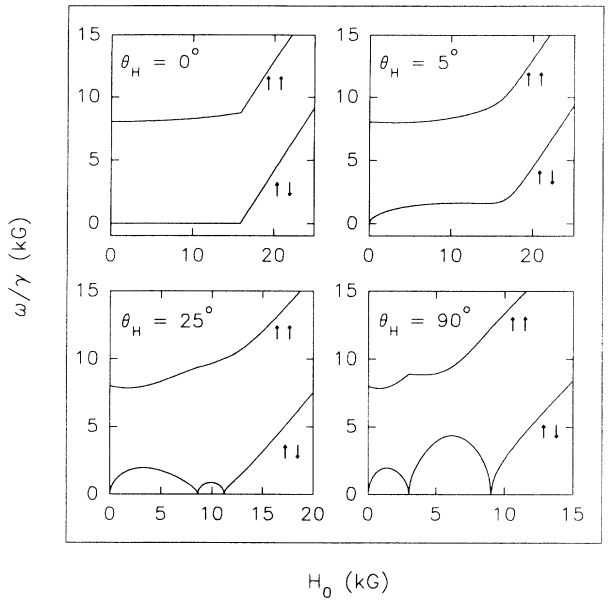

FIG. 6. The dispersion relation for an asymmetrical trilayer system with the external field applied at different orientations. The parameters are the same as those used in Fig. 2.

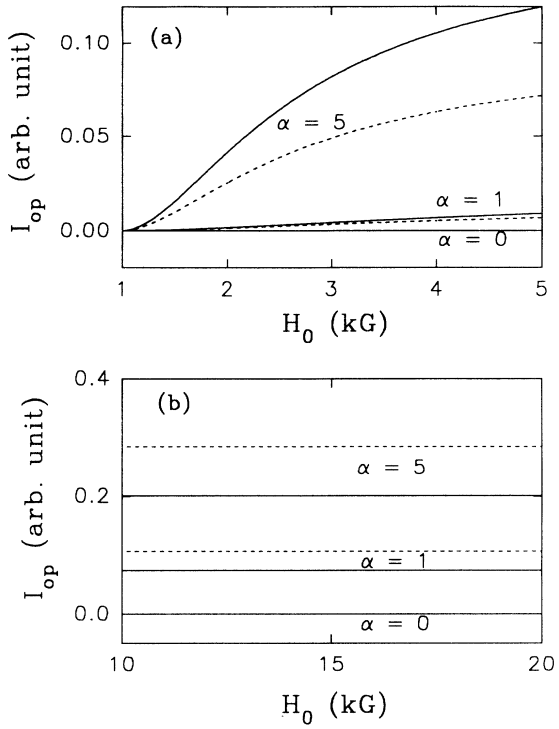

FIG. 7. The intensity of the optic mode I_{op} as a function of the resonance field for different α values which measures the ratio between the difference in the anisotropy field $H_{u2,i}^{\text{eff}}$ and the exchange field H_{ex}. The external field is applied either in the film plane (a) or perpendicular to the film (b). The systems are chosen so that the in-plane and out-of plane saturation fields are constant at 1 and 10 kG, respectively. The solid lines correspond to $t_1=t_2$ system and the dashed lines correspond to $t_1=2t_2$.

$\theta_H > \theta_{\text{cri},1}$, the feature of the dispersion relation curve remains essentially the same except that the singularities change their positions. This suggests that the transition at $\theta_H=\theta_{\text{cri},2}$ is a higher-order effect. When the external field is applied in the film plane, there is no crossover point in contrast to the symmetrical system (Fig. 4). Instead, the upper branch and the lower branch are separated by an energy gap which will exist over the whole range of θ_H.

C. Absorption intensity

In order to observe the ferromagnetic resonance mode, the system must have a net rf component of the magnetic moment along the pumping field direction. The intensity of the microwave absorption can be expressed as[16]

$$I \propto \frac{(t_1 m_{h,1}+t_2 m_{h,2})^2}{(t_1+t_2)[t_1(m_{\theta_1}^2+m_{\phi_1}^2)+t_2(m_{\theta_2}^2+m_{\phi_2}^2)]} , \tag{10}$$

where $m_{h,1}$ and $m_{h,2}$ are the rf component of the magnetization along the pumping field direction in layers 1 and 2, respectively.

When the magnetization vectors are saturated at the resonance condition, the rf component of the magnetic moment in each layer resonates either in phase (acoustic mode) or out of phase (optic mode). The in phase (acoustic) mode will produce a relatively large microwave absorption because $m_{h,1}$ is always parallel to $m_{h,2}$. For the optic mode, the intensity is relatively small due to the opposite sign of $m_{h,1}$ and $m_{h,2}$ and when the two layers have the same anisotropy fields (i.e., $H_{u2,1}^{\text{eff}}=H_{u2,2}^{\text{eff}}$ and $H_{u4,1}=H_{u4,2}$), the intensity of the optic mode will be zero.

In general, the intensity of the optic mode depends on the ratio between the difference in the internal anisotropy field and the exchange-coupling field,

$$\alpha=\frac{|H_{u2,1}^{\text{eff}}-H_{u2,2}^{\text{eff}}|}{A_{12}(t_1+t_2)/t_1 t_2 M_s} , \tag{11}$$

as well as the direction at which the field is applied and the resonance frequency (or resonance field). As an example, in Fig. 7, the variation of the optic mode absorption as a function of the resonance field is shown for the parallel ($\theta_H=90°$) and perpendicular ($\theta_H=0°$) orientations. The higher-order uniaxial anisotropy field $H_{u4,i}$ is usually small in comparison with $H_{u2,i}^{\text{eff}}$ and is assumed zero for this calculation. It can be seen that at each orientation, the intensity of the optic mode increases with increasing α value. For a given film having a fixed value of α, the optic mode is much easier to be observed in the perpendicular orientation than in the parallel orientation. If the field is applied perpendicular to the film, the intensity of the optic mode is independent of the microwave frequencies (or magnetic resonance field). However, if the field is applied parallel to the film, the higher the resonance frequency (or larger resonance field), the larger the optic mode absorption. This frequency-dependent absorption is related to the change of the resonance ellipticity, m_{θ_i}/m_{ϕ_i}, with frequency (or field).

The change of the microwave absorption with α, θ_H, and frequency can be very useful in evaluating the exchange coupling in multilayer systems. As an example, if a system has a large α value, it might be difficult to distinguish the acoustic mode and the optic mode in the perpendicular FMR spectra because both modes will have similar microwave absorption. However in the parallel FMR spectra, the intensity of the optic mode may be significantly reduced, making it possible to distinguish the two modes. If a system has a small α value, the optic mode in the parallel FMR spectra might be too weak to be detected. In this case, the perpendicular FMR spectra might be the desired orientation to observe the optic mode.

When the system is unsaturated, the resonance mode cannot be catalogued as either an acoustic mode or an optic mode except for very few special cases (for example, the parallel and perpendicular resonance spectra as shown in Fig. 3). The intensity of each mode is sensitive to many resonance parameters and does not always follow such common rules as discussed in the saturated configuration.

D. Longitudinal pumping

From the calculation of the dispersion relation, it can be seen that the observation of the optic mode is very important for the evaluation of A_{12}. However, the intensity of this mode is very small for most of the systems and zero for symmetrical systems. Also the linewidth of this mode is usually larger than that of the acoustic mode due to the fluctuation of A_{12} across the film plane. All of these factors limit the accuracy with which the resonance field of the optic mode can be determined.

One method to overcome this difficulty is to use the angular dependence of the main resonance mode in the unsaturated state of an antiparallel coupled system. However, due to the energy gap in Fig. 5, this main mode might not exist when θ_H is less than a certain value. The angle $\theta_H = \theta_d$ at which the signal starts to disappear is crucial for the determination of A_{12} but is often difficult to obtain accurately due to the sudden broadening of the linewidth with the angle and the rapid decrease of the intensity of the signal when θ_H is approaching θ_d.

The other method is to increase the α value by changing the thickness of one of the ferromagnetic layers,[8] therefore increasing the intensity of the optic mode. However, even with the condition that the second ferromagnetic layer is about half as thick as the first magnetic layer ($\sim$10 Å), the intensity of the optic mode is still relatively weak.[8] Another problem associated with the change of the ferromagnetic layer thickness is that the interlayer exchange coupling strength might also change even for the same spacer thickness.[18,19]

The optic mode can be observed handily even for the symmetrical systems if the rf pumping field is applied along the bias field orientation (longitudinal pumping). In order to get a longitudinal pumping signal, the system must be in the unsaturated state and have a rf component of the magnetization along the bias field direction. Figure 8 shows a schematic diagram of both the transverse and longitudinal pumping geometry for a symmetrical trilayer system with the bias field applied in the film plane. When the pumping field $\mathbf{h}_0$ is perpendicular to the bias field $\mathbf{H}$, only the acoustic mode has a net rf moment along the $\mathbf{h}_0$ direction and can be observed. However, when $\mathbf{h}_0$ is parallel to $\mathbf{H}$, the optic mode is coupled to the rf field and produces a microwave absorption. If $\mathbf{h}_0$ is applied at an intermediate angle with respect to $\mathbf{H}$, both the acoustic mode and the optic mode can be observed in the same spectra. An experimental verification of this effect is shown in Fig. 8. Since $\mathbf{H}$ is always in the film plane, the positions of the acoustic mode and the optic mode do not change with the rotation of $\mathbf{H}$.

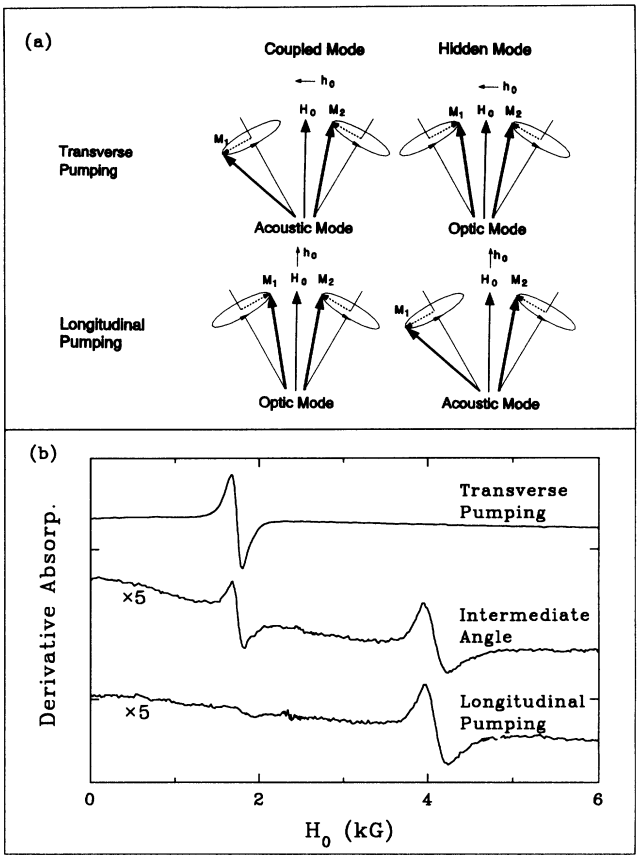

FIG. 8. (a) A schematic diagram of longitudinal and transverse pumping in the FMR setup. $\mathbf{h}_0$ and $\mathbf{H}_0$ are microwave pumping field and bias field, respectively. $\mathbf{M}_1$ and $\mathbf{M}_2$ are magnetization vectors in magnetic layers 1 and 2, respectively. (b) The in-plane FMR spectra of the Co(32 Å)/Ru(9.5 Å)/Co(32 Å) sample at X-band frequency and room temperature. The rf field is applied at 90° (top), 20° (middle), and 0° (bottom) with respect to the bias field.

III. EXPERIMENTAL RESULTS

A. Growth and characterization

The Co/Ru/Co samples were prepared in ultrahigh vacuum ($\sim 5\times10^{-11}$ Torr before deposition, $\sim 5\times10^{-10}$ Torr during deposition) by evaporation on freshly cleaved mica substrates. A thick epitaxial Ru layer (150 Å) was

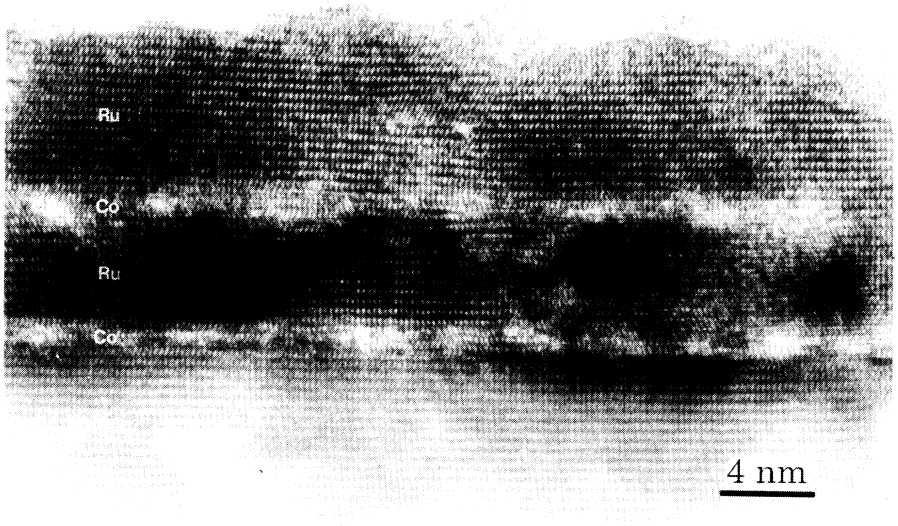

FIG. 9. Cross-sectional high-resolution TEM image of the Co(12 Å)/Ru(35 Å)/Co(12 Å) trilayer structure [from G. Pan (Ref. 21)].

deposited on mica as a buffer layer and was followed by the Co/Ru/Co trilayer structure. Another Ru layer (40 Å) was then deposited on the top of the film as a protection layer. Despite the large lattice mismatch ($\sim 8\%$), the RHEED patterns obtained during the sample growth and scanned over the whole surface show extensive coherency of the surface and reveal high crystalline quality.[20] The high-angle x-ray diffraction on the Co/Ru superlattices evidenced the composition modulation and the long-range structure coherence even for very thin Ru layers. The rocking curve of the main superlattice Bragg peak shows a slight spread of the c-axis orientation of about 1.5°. Transmission electron microscopy (TEM) studies confirmed the hcp structure for both Co and Ru layers with a strain relaxation for Co thicknesses larger than 15 Å. The layers are epitaxially grown on the Ru buffer layer with good crystalline features as shown on TEM cross sections (Fig. 9).[21]

Several series of samples have been investigated and their structures are listed in Table I. In the first and second series, the thickness of each Co layer is constant at 32 Å (symmetrical structure) while the Ru layer thickness varies from 6 to 80 Å. The purpose of this study is to investigate the interlayer exchange coupling as a function of the Ru spacer thickness. The only difference between series I and II is the substrate temperature during film deposition. In the first series of samples, the substrate temperature was kept at 120 °C. The RHEED patterns in these samples indicate that the first Co layer on the Ru buffer follows a monolayer by monolayer growth mechanism while the crystal structure of the second Co layer has a significantly larger number of stacking defaults.[20] As a result, the internal uniaxial anisotropy fields in the second Co layer differ from those in the first layer even though the layer thickness is the same.

In order to improve the growth properties of the second Co layer, the deposition temperature was reduced to a much lower value (< 0 ° C) in the second series. By doing that, the crystal structure of the second Co layer is almost as good as that of the first Co layer in this series, therefore a much smaller difference in the anisotropy field is expected between the two Co layers.

The deposition temperature for series III–V was also kept at the sam temperature as that for the second series. In each of these three series, the Ru layer thickness t_{Ru} is constant while the thickness of the second Co layer varies from 8 to 32 Å. $t_{Ru} = 10$ Å, 12, and 16 Å for series III, IV, and V, respectively. The motivation for these series is (i) to create an asymmetric anisotropy environment for the observation of the optic mode and (ii) to systematically investigate the variation of the interlayer exchange coupling with the magnetic layer (Co) thickness.

B. Magnetization measurements

Magnetization measurements were performed using a SQUID and an AGFM (alternating gradient force magnetometry) magnetometers at room temperature and low

TABLE I. Structure characterizations of the Co/Ru/Co films.

Series	Structure	Variable thicknesses (Å)	Deposition temperature (°C)
I	Co(32 Å)/Ru(t_{Ru})/Co(32 Å)	9.5, 12, 16, 20, 24, 28, 32, 80	120
II	Co(32 Å)/Ru(t_{Ru})/Co(32 Å)	6, 7, 9, 10.5, 11, 14	−30
III	Co(32 Å)/Ru(10 Å)/Co(t_2)	6, 8, 11, 14, 16, 19, 21, 22, 26, 29, 32, 35	−30
IV	Co(32 Å)/Ru(12 Å)/Co(t_2)	6, 10, 11, 13, 14, 16, 18, 21, 24, 27, 30, 32	−30
V	Co(32 Å)/Ru(16 Å)/Co(t_2)	8, 10, 11, 13, 14, 16, 18, 21, 24, 27, 30, 32	−30

temperatures. Except for $t_2 < 10$ Å in the asymmetrical Co(32 Å)/Ru(t_{Ru})/Co(t_2) structures, all samples have easy-plane anisotropy energy. The magnetic moment per unit volume of Co is within 10% of the bulk Co value (1400 emu/cm^3) and is independent of both the Ru thickness (in the symmetrical structures) and the second Co layer thickness (in the asymmetrical structures). The largest source of error for the evaluation of the magnetization M_s comes from the uncertainty in the layer thickness influencing the volume calculation of Co within the sample. Therefore, the magnetization of the bulk Co value is used as M_s inside each Co layer.

No significant in-plane anisotropy field was found as expected for the hcp structure in the Co and Ru layers having the c axis normal to the film plane.[20] The systems which show nearly square hysteresis loops around zero magnetic field are assumed to be parallel coupled or noncoupled. Other systems which require much larger applied fields to be saturated are considered as antiparallel coupled systems. The in-plane saturation field for an antiparallel coupled system is calculated by extrapolating the slope of the magnetization curve in the unsaturated (canted) region to the saturation value of M_s.

1. *Symmetrical structures*

The in-plane magnetization measurements for the symmetrical structures (series I and II) are shown in Fig. 10. Oscillations of the saturation field as a function of the Ru thickness were observed. The two Co layers are antiparallel coupled in the regions $8 < t_{Ru} < 12$ Å and $20 < t_{Ru} < 24$ Å. The maximum coupling strength in the first antiparallel coupled region, which corresponds to an in-plane saturation field $H_{sat,\parallel} \sim 8$ kOe at $t_{Ru} = 9$ Å, is much larger than that in the second antiparallel coupled region ($H_{sat,\parallel} \sim 0.5$ kOe).

In the very thin Ru samples (Ru 6- and 7-Å samples), a large in-plane field (maximum value of about 20 kOe) is required to saturate the sample, indicating that the magnetization vectors of the two Co layers are strongly antiparallel coupled for extremely thin Ru spacer. This agrees with the theoretical predication from *ab initio* band-structure calculation.[22] However, the shape of the hysteresis loop differs from that of an ideal antiparallel coupled system, showing rapid increase of the induced magnetic moment for small magnetic field and a rather long tail as the induced magnetization reaches its satura-

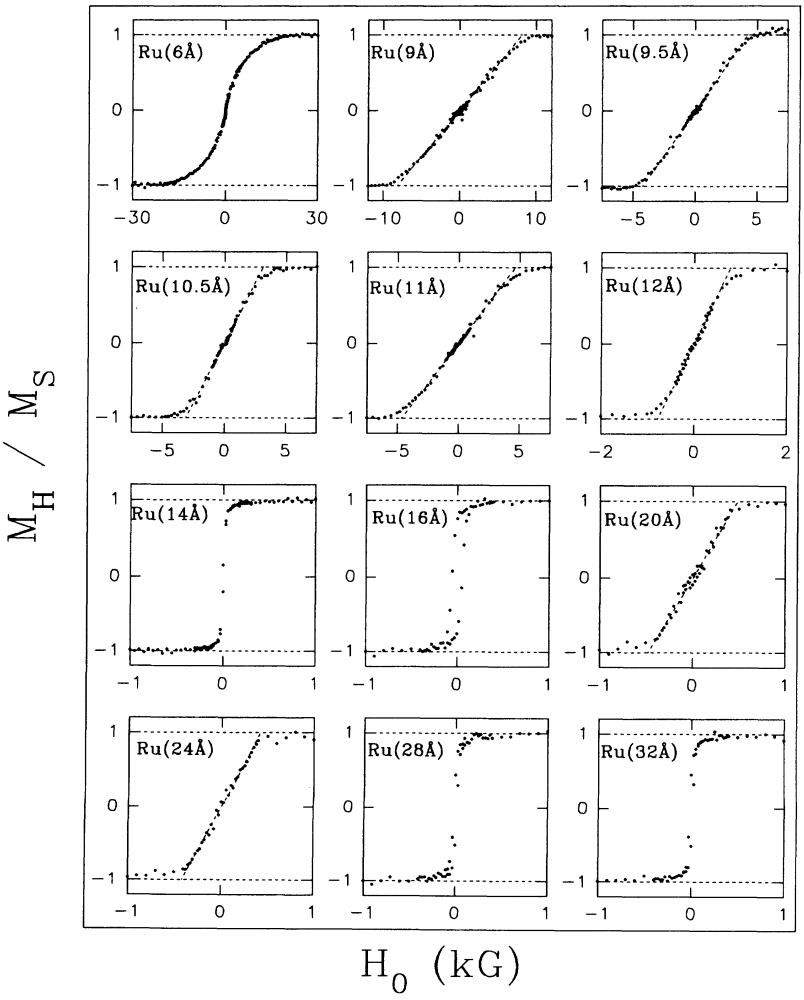

FIG. 10. In-plane magnetization curves for the symmetrical Co(32 Å)/Ru(t_{Ru})/Co(32 Å) structures (series I and II) at room temperature.

tion value (see Fig. 10). This suggests the existence of a large variation in the interlayer exchange coupling which may be due to pinhole formation and the fluctuation of the Ru layer thickness across the film. Moreover, nuclear magnetic resonance experiments[23] and magnetization measurements[24] on a series of single Co layer deposited on the Ru buffer layer with various Co thickness from 4 to 30 Å have evidenced an intermixing of Co and Ru across two atomic planes at the interface, in agreement with the structure analysis.[20]

The temperature dependence of the in-plane magnetization measurement has been performed on some of the antiparallel coupled films. With decreasing temperature, the magnetization in each Co layer increases slowly—for example, from 1300 emu/cm^3 at 300 K to 1400 emu/cm^3 at 100 K for the sample Co(32 Å)/Ru(9 Å)/Co(32 Å). The in-plane saturation field also increases with decreasing temperature—from ~8 kOe at room temperature to ~10 kOe at 100 K for the same sample. This behavior indicates an increase in the exchange coupling strength $|A_{12}|$ at low temperatures.

2. Asymmetrical structures

Series III and IV, which have the asymmetrical structures Co(32 Å)/Ru(t_{Ru})/Co(t_2) with $t_{Ru}=10$ and 12 Å respectively, show typical antiparallel exchange-coupled

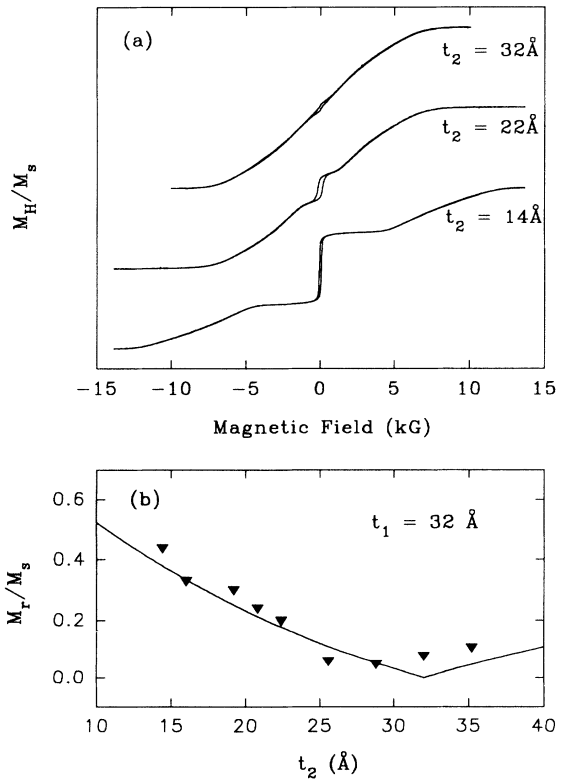

FIG. 11. (a) Typical in-plane magnetization curves for the asymmetrical Co(32 Å)/Ru(10 Å)/Co(t_2) samples at room temperature. (b) The remanent magnetization M_r (in units of M_s) as a function of the second Co layer thickness t_2 for this series. The curve is the calculation using the relation $M_r/M_s=|(t_1-t_2)/(t_1+t_2)|$.

magnetization curve as predicted in Fig. 2(d). Upon decreasing the thickness of the second Co layer t_2, the remanent magnetization increases and follows roughly the relation $M_r/M_s=(t_1-t_2)/(t_1+t_2)$ as shown in Fig. 11. This provides the evidence about the quality of the system and the consistency of the layer thickness from sample to sample. The well-defined shape of the hysteresis loops also indicates that the interlayer exchange coupling is quite uniform across the film plane.

In the Co(32 Å)/Ru(16 Å)/Co(t_2) series, a nearly square hysteresis loop is obtained for all of the samples. The in-plane saturation field is less than 100 Oe and does not vary significantly from sample to sample, suggesting that the Co layers are not antiparallel coupled in this series as opposed to the other two asymmetrical series.

C. Ferromagnetic resonance

Several different FMR experiments have been applied to the Co/Ru/Co trilayer structures. (i) The resonance frequency can be at either X band (9.2 GHz) or K band (23 GHz). (ii) The external field can be applied at an arbitrary angle with respect to the film plane, i.e., $0°\leq\theta_H\leq 90°$. (iii) The temperature can vary from 10 to 300 K. (iv) When the external bias field is applied in the film plane, the rf pumping field can be either parallel (longitudinal pumping) or perpendicular (transverse pumping) to the bias field. Due to the change of the experimental configurations, the resonance spectra can be significantly different from one to the other configurations even for the same sample. In this section, some typical resonance spectra and their variation with θ_H and temperature will be given for both the parallel and antiparallel coupled systems.

1. Symmetrical structure

Figure 12 shows the in-plane FMR spectra at room temperature for some of the samples in series I. Two resonance modes were observed in most of the samples in this series. Except for the resonance mode of the sample $t_{Ru}=9.5$ Å, the field positions of the strong acoustic mode are nearly constant for all of the samples at a given frequency. The weak optic mode, however, changes its position between the higher and the lower field side of the acoustic mode with the change of the Ru thickness.

When the external field is applied perpendicular to the film, the FMR spectra become more complicated. At X band, two resonance modes were observed in all samples except in the $t_{Ru}=9.5$ Å sample in which only the acoustic mode was obtained. Typical spectra are shown in Fig. 13. All of the samples shown in this figure have their weak optic mode on the high-field side of the acoustic mode in the parallel FMR spectra. However, for the $t_{Ru}=20$ and 24 Å samples, the intensities of the optic mode and acoustic mode are almost equal in the perpendicular spectra. It was also observed that the separation between the two modes in much larger in the perpendicular spectra than that in the parallel spectra for these two samples.

In the second series of samples, only the acoustic mode

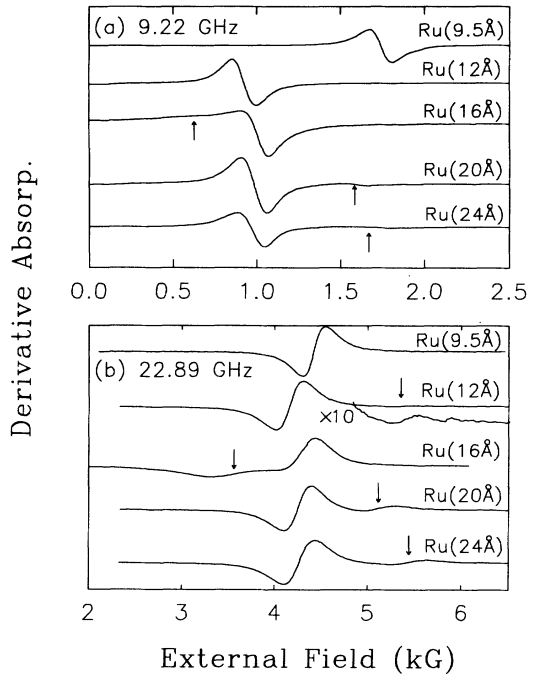

FIG. 12. In-plane FMR spectra at X-band (a) and K band (b) for some of the Co(32 Å)/Ru(t_{Ru})/Co(32 Å) samples in series I at room temperature. The arrows indicate the positions of the optic modes under high resolution.

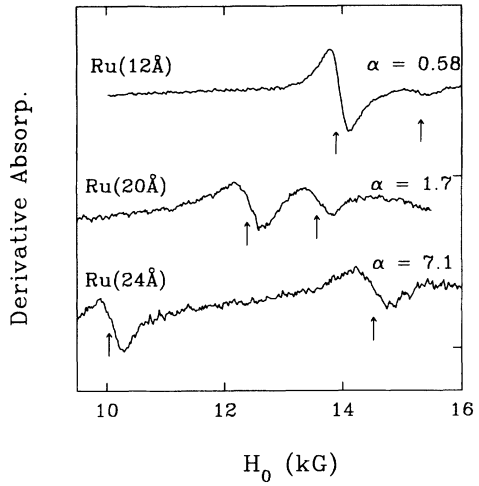

FIG. 13. Perpendicular FMR spectra at X band for some of the antiparallel coupled Co(32 Å)/Ru(t_{Ru})/Co(32Å) samples in series I at room temperature. The arrows indicate the positions of the resonance modes. α was calculated using the method described in the text.

was observed in the FMR spectra at X-band and K-band frequencies.

For the samples listed in Table II, a critical angle θ_d exists in the X-band FMR spectra when the external field is rotated continuously from the parallel ($\theta_H=90°$) to the perpendicular orientation ($\theta_H=0°$). At $\theta_H=90°$, a strong resonance mode is observed. The position of the resonance field increases with decreasing θ_H. As θ_H is approaching the value of θ_d, the linewidth of the signal becomes very broad and the intensity of the signal decreases dramatically. When θ_H is smaller than θ_d, this mode cannot be observed in the FMR spectra. The typical variation of the resonance field with θ_H is shown in Fig. 14(a).

θ_d does not exist in the K-band FMR spectra. However, unlike other samples listed in Table II, the resonance behavior for the Co(32 Å)/Ru(9 Å)/Co(32 Å) sample is significantly different from that of a single-layer films. The resonance field of this sample remains at relatively low values (between 5.5 and 7.2 kOe) during the whole range of rotation. A maximum resonance field with the value of 7.2 kOe was obtained when the angle of the external field, θ_H^{max}, is about 20° off from the perpendicu-

TABLE II. Room-temperature magnetic properties of the four strongly antiparallel coupled Co(32 Å)/Ru(t_{Ru})/Co(32 Å) films as described in the text.

Series	t_{Ru} (Å)	H_{ex} (kG)	g-value	H_{2u}^{eff} (kG)	Critical angle at X band Prediction (deg)	Experiment (deg)
II	9	8.7	2.22	−5.8	24	25
I	9.5	4.59	2.18	−9.58	16	15
II	10.5	4.87	2.22	−8.16	21	20
II	11	5.18	2.16	−8.31	22	25

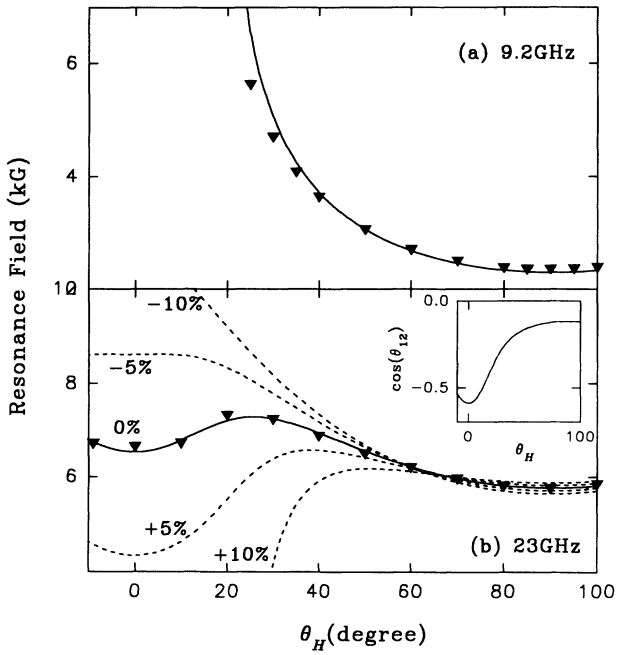

FIG. 14. Angular dependence of the resonance field for the Co(32 Å)/Ru(9 Å)/Co(32 Å) sample at X-band (a) and K band (b) frequencies and room temperature. The solid lines are theroetical fits using the same parameters as in Fig. 4. The dashed lines in (b) are predictions corresponding to 5 and 10% changes in the exchange field H_{ex}. The inset of (b) is the variation of $\cos(\theta_{12})$ with θ_H at the K-band resonance condition, where θ_{12} is the angle between $\mathbf{M}_1$ and $\mathbf{M}_2$. A constant A_{12} used in this fit indicates that the biquadratic exchange term B_{12} is negligible in this sample.

lar orientation as shown in Fig. 14(b). Upon decreasing the temperature, $\theta_H^{\max}$ increases from 20° at 300 K to about 80° at 50 K. The resonance field in the perpendicular orientation does not change significantly with temperature (from 6.2 to 6.5 kOe), however, the parallel resonance field increases from 5.7 to 6.7 kOe as the temperature decreases from 300 to 50 K.

For all of the samples listed in Table II, the optic mode was observed using the longitudinal pumping technique at X-band frequencies (see Fig. 8). The linewidth of the optic mode is on the order of 250 G for all of the samples. The positions of both the acoustic mode and the optic mode increases with decreasing temperature.

2. *Asymmetrical structures*

In the two antiparallel coupled asymmetrical structure, only the acoustic mode is observed. However, in the parallel coupled asymmetrical series having the structure of Co(32 Å)/Ru(16 Å)/Co(t_2), both the acoustic and the optic modes are observed at X-band and K-band frequencies. A typical variation of the resonance field with θ_H is shown in Fig. 15. With increasing θ_H, one mode always stays on the lower field side of the other mode. This is opposed to the behavior of a noncoupled asymmetrical trilayer structure where a crossover point would be obtained.

IV. ANALYSIS

Using the resonance theory discussed in Sec. II, the interlayer exchange-coupling strength and the uniaxial anisotropy fields can be evaluated from the FMR data for both the parallel and antiparallel coupled system. For the antiparallel coupled system, the in-plane magnetization measurements can be used to determine the value of A_{12}.

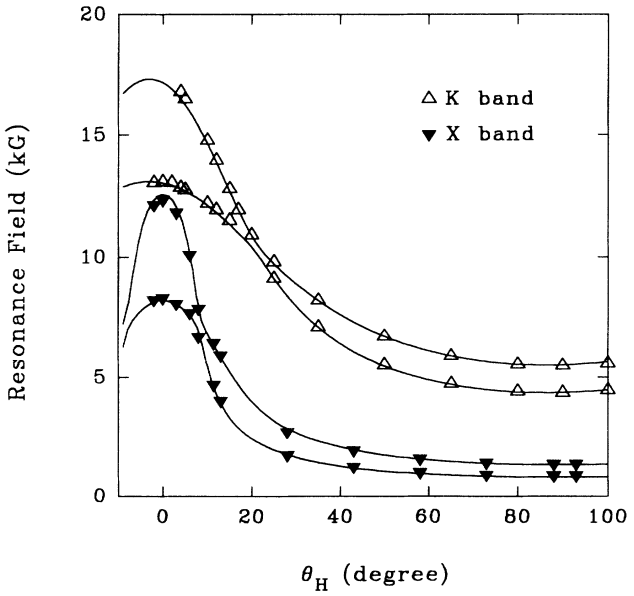

FIG. 15. Angular dependence of the resonance field for the Co(32 Å)/Ru(16 Å)/Co(18 Å) sample at X-band and K-band frequencies and room temperature. The solid lines are best fit using the parameters $H_{u2,1}^{\text{eff}} = -9.50$ kG, $H_{u2,2}^{\text{eff}} = -5.36$ kG, $g = 2.09$, and $A_{12} = -0.045$ erg/cm^2.

A. Variation of A_{12} with the Ru layer thickness (t_{Ru})

Due to the different growth quality between the first and second Co layer in series I, a difference in the internal anisotropy field is developed in each layer and both the acoustic mode and the optic mode were observed in the FMR spectra. The optic mode is on the higher field side of the acoustic mode for the samples with the Ru thickness at 12, 20, and 24 Å, indicating that in zero magnetic field the magnetization vectors of the two Co layers are antiparallel coupled for these samples. This agrees with the results from the in-plane magnetization measurement shown in Fig. 10. The resonance of the Co(32 Å)/Ru(16 Å)/Co(32 Å) sample has the optic mode on the low-field side of the main mode, indicating a weak parallel exchange coupling between the Co layers. From Fig. 12, the intensity of the optic mode in the K-band spectra is larger and easier to be detected than that in the X band, in agreement with the previous predictions that the relative intensity of the optic mode increases with the increase of the microwave frequency (see Fig. 7).

In contrast to the parallel spectra, the intensity of the optic mode in the perpendicular orientation changes significantly from one to the other (as shown in Fig. 13). In addition, for most of the samples shown in Fig. 12, the separation between the optic mode and the acoustic mode is much larger at the perpendicular orientation than that at the parallel orientation. This is consistent with a 1–3 kG difference in the anisotropy fields between the two Co layers, $|H_{u2,1}^{\text{eff}} - H_{u2,2}^{\text{eff}}|$, which gives a significant contribution to the field separation in the perpendicular resonance spectra (about the same order as $|H_{u2,1}^{\text{eff}} - H_{u2,2}^{\text{eff}}|$) as opposed to about a 0.1-kG contribution to the separation in the parallel spectra.

From the resonance fields in both the parallel and the perpendicular resonance spectra, A_{12} and $H_{u2,i}^{\text{eff}}$ were accurately determined for all the samples shown in Fig. 12 except the $t_{\text{Ru}} = 9.5$ Å samples. The calculated α value for each sample agrees with the predictions that the larger the α value is, the larger the intensity of the optic mode is as clearly shown in Fig. 13.

For the Co(32 Å)/Ru(9.5 Å)/Co(32 Å) sample, only one mode was observed as opposed to the two modes in other samples of the same series. The in-plane resonance field at K band is close to that of the other samples, suggesting that all of the films have similar uniaxial anisotropy fields, H_{u2}^{eff}, which is about -9 kG in average. However at X-band frequency, the resonance field for the Co(32 Å)/Ru(9.5 Å)/Co(32 Å) sample is much higher (about 1.7 kOe) than the 1.0 kOe observed in other samples, but lower than its saturation value ($H_{\text{sat},\parallel} \sim 4$ kOe). This novel shift in the resonance spectra is due to the smaller contributions of the demagnetization energy in the unsaturated state as predicted from the theoretical calculation (Fig. 4). In the perpendicular FMR spectra at X band, only one weak mode was observed at $H \sim 16$ kOe. This mode has been identified as the optic mode because the resonance field is so much higher than that of the acous-

tic mode found in the other samples. Using the 4 and -9 kG as estimations for H_{ex} and H_{u2}^{eff}, the main (acoustic) mode falls in the frequency gap at the perpendicular orientation at X-band frequencies. This supports the observation that the main mode disappears for $\theta_H < \theta_d$ for this sample as shown in Fig. 14(a).

Because of the strong antiparallel coupling in the Co(32 Å)/Ru(9.5 Å)/Co(32 Å) sample, the longitudinal pumping technique was applied for the observation of the optic mode at X-band frequency. The narrow linewidth of the optic mode (about 250 Oe in comparison with the resonance field at about 4 kOe) does not necessarily indicate that the variation of A_{12} is very small across the film plane. Instead, it suggests that the variation length (along the film plane) in these Co/Ru/Co trilayer films is much smaller than the magnetic correlation length of bulk Co (domain-wall width, about 1000 Å) because the linewidth of the resonance spectra, in this case, is significantly reduced by a factor of $\Delta A_{12}/A_{Co}$ as predicted in the literature.[25] Here A_{Co} is the direct exchange energy coefficient in the bulk Co and is much larger than A_{12}.

The exchange-coupling strength for this sample is evaluated using the optic mode at X band and the acoustic mode at both the X-band and K-band frequencies. This evaluation method has also been applied to the $t_{Ru}=9$, 10.5, and 11 Å samples in series II, all of which have in-plane saturation field of 3 kOe or larger. Since no optic mode was observed in these samples using the transverse pumping technique, the two Co layers are assumed to have the same anisotropy field. The parameters, A_{12}, H_{u2}^{eff}, and g value, determined from this method successively predict the angular dependence of the FMR data at both the X-band and K-band frequencies (Fig. 14). The critical angle θ_d predicted for the X-band resonance behavior agrees with the experimental data as shown in Table II. Except for $t_{Ru}=9$ Å, all samples are saturated under K-band resonance condition, therefore the angular dependence of the main (acoustic) mode follows the same variation as that of a single layer system.

For the $t_{Ru}=9$ Å sample, the antiparallel exchange field is so large (>8 kG) that the magnetic moment is not saturated even at the K-band frequency. From the calculated dispersion relation (Fig. 4), it can be seen that the resonance mode observed in the K-band spectra is associated with the intercept of the frequency to the upper dispersion curve in the unsaturated region. When the external field is applied close to the perpendicular orientation the slope near the resonance field is much smaller than that in the saturated region, suggesting that a small variation in the shape of the dispersion curve will change the K-band resonance field significantly for this sample. As an example, the deviations corresponding to 5 and 10% changes in the exchange coupling field, H_{ex} are shown as the dotted lines in Fig. 14(b). From this analysis, it can be seen that the error of evaluating A_{12} and H_{u2}^{eff} is within 1%. Since the angle between $\mathbf{M}_1$ and $\mathbf{M}_2$ at resonance changes with θ_H [see the inset of Fig. 14(b)], the fit of the calculation to the experimental data also indicates that the biquadratic exchange energy is at least 2 orders of magnitude smaller than the bilinear term in the Co/Ru/Co trilayer series.

The interlayer exchange coupling coefficient A_{12} as a function of the Ru thickness is shown in Fig. 16. The evaluation of A_{12} from the in-plane saturation field, $H_{sat}=2A_{12}/t_{Co}M_s$, is also shown for comparison. A_{12} oscillates from positive to negative values with respect to the Ru thickness, having a long oscillation period of about 10 Å. The magnetization vectors of the two Co layers are strongly antiparallel coupled with the coupling field on the order of several kG for $8 \le t_{Ru} \le 12$ Å, in agreement with the previous results in the literature.[10] A maximum exchange coefficient A_{12} with a value of 1.85 erg/cm^2 was found in the sample $t_{Ru}=9$ Å, which corresponds to an exchange field H_{ex} of 8.3 kG. The maximum coupling strength in the second antiparallel coupled region ($20 < t_{Ru} < 24$ Å) is at least an order of magnitude smaller than that in the first antiparallel coupled region.

The existence of parallel exchange coupling was confirmed in the sample $t_{Ru}=16$ Å from the FMR data. The exchange field $|H_{ex}|$ for this sample is about 0.3 kG, even smaller in magnitude than the maximum values in the second antiparallel coupled region ($20 < t_{Ru} < 24$ Å). In addition, the range of the parallel coupling region is smaller than those of the antiparallel coupling regions. For the samples with Ru thickness greater than 28 Å, the amplitude of the exchange coupling $|A_{12}|$ is less than 0.05 erg/cm^2 and cannot be detected by the FMR technique.

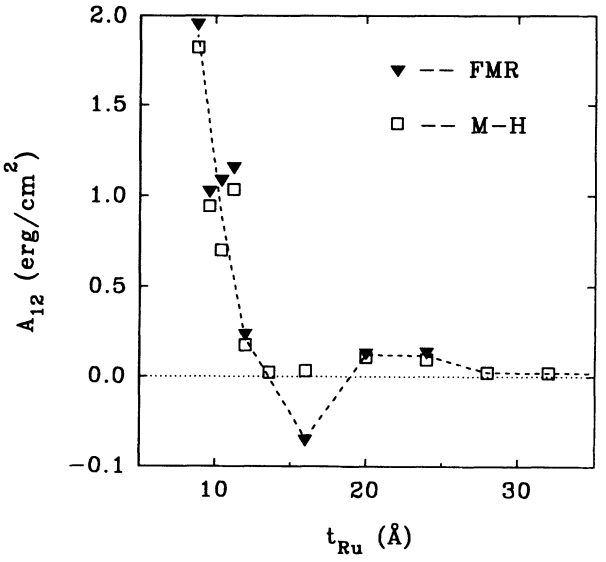

FIG. 16. The evaluation of the exchange-coupling strength A_{12} as a function of the Ru thickness t_{Ru} for the symmetrical Co(32 Å)/Ru(t_{Ru})/Co(32 Å) structures at room temperature. The solid triangles are the fitting results from the FMR analysis while the open squares are the evaluation from the in-plane saturation fields. The scale of the y axis below zero is expanded.

B. Temperature dependence of A_{12}

To further explore the exchange-coupling mechanism in the magnetic multilayer system, the temperature dependence of FMR has been performed on four samples in the symmetrical structures having the Ru thickness of 9, 9.5, 20, and 24 Å, respectively. All of these samples have antiparallel exchange coupling between the Co layers at room temperature. The $t_{Ru}=9$ and 9.5 Å samples are in the first antiparallel coupled region while the $t_{Ru}=20$ and 24 Å samples are in the second antiparallel coupled region.

For the $t_{Ru}=9$ Å sample, A_{12} is evaluated from the angular dependence of the resonance field at the K-band frequency. Although the in-plane magnetization measurement indicates a 20% increase of the saturation field with decreasing temperature from 300 to 100 K, the perpendicular resonance field does not change significantly over this temperature range as opposed to the prediction in Fig. 14(b). This is due to the change in the anisotropy field within each Co layer which nearly compensates for the increasing in the exchange coupling in the perpendicular orientation but it gives a significant increase to the parallel resonance field, from 5.6 kOe at room temperature to 6.6 kOe at 50 K.

For the $t_{Ru}=9.5$ Å sample, the longitudinal pumping technique was used for the temperature-dependence study. With decreasing temperature, the resonance fields of both the acoustic mode and the optic mode increases, suggesting an increase of the exchange coupling strength and a decrease of $|H_{u2}^{\text{eff}}|$ at low temperatures.

For the $t_{Ru}=20$ and 24 Å samples, the exchange-coupling strength was evaluated from the field separation between the acoustic mode and the optic mode in the parallel FMR spectra at X band. Due to the difference in the effective anisotropy field between the two Co layers, $|H_{u2,1}^{\text{eff}}-H_{u2,2}^{\text{eff}}|\neq 0$, the field separation between these two modes, in general, is equal to the exchange field H_{ex} plus a correction due to $|H_{u2,1}^{\text{eff}}-H_{u2,2}^{\text{eff}}|\neq 0$. However, evaluating the results at room temperature, it was found that the contribution of the later term is insignificant for these two samples. Therefore, the field separation is used as an approximation for the exchange-coupling field H_{ex}.

The temperature dependence of the interlayer exchange coupling is shown in Figs. 17 and 18 for these samples. With decreasing temperature, A_{12} increases, suggesting that the oscillatory exchange coupling shown in Fig. 16 does not change its oscillation period or phase, but rather changes its oscillation amplitude with temperature. Except for the $t_{Ru}=24$ Å sample, the variation of A_{12} with temperature follows the relationship

$$A_{12}=A_{12}(0)\frac{T}{T_0}\Big/\sinh\left[\frac{T}{T_0}\right] \tag{12}$$

predicted by Edwards *et al.*[26] and Bruno *et al.*[27] (shown by the solid lines in Figs. 17 and 18). For the $t_{Ru}=24$ Å sample, only the data below 120 K can be fit to Eq. (12). The high-temperature data are significantly larger than the theoretical predictions as shown by the solid line in Fig. 18(b). This behavior is opposed to the expectation

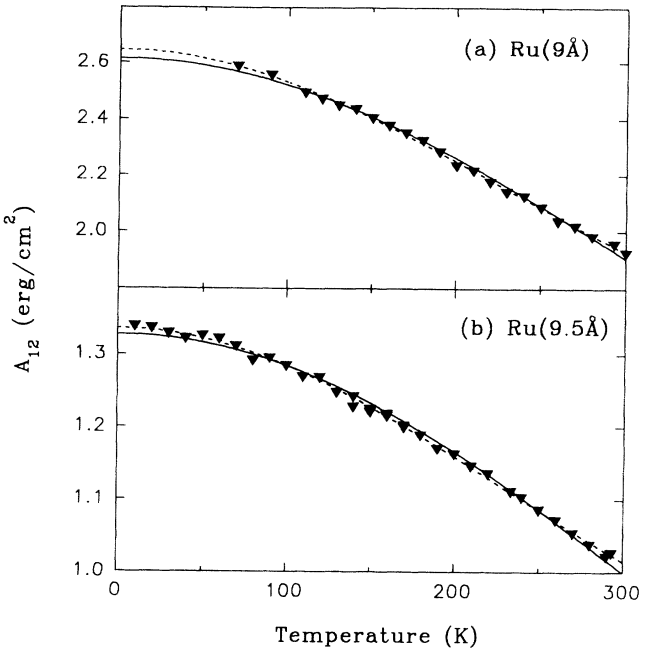

FIG. 17. The evaluation of A_{12} as a function of temperature for (a) the Co(32 Å)/Ru(9 Å)/Co(32 Å) and (b) the Co(32 Å)/Ru(9.5 Å)/Co(32 Å) samples. The solid lines and the dashed lines are best fits using Eqs. (12) and (13), respectively, with the parameters listed in Table III.

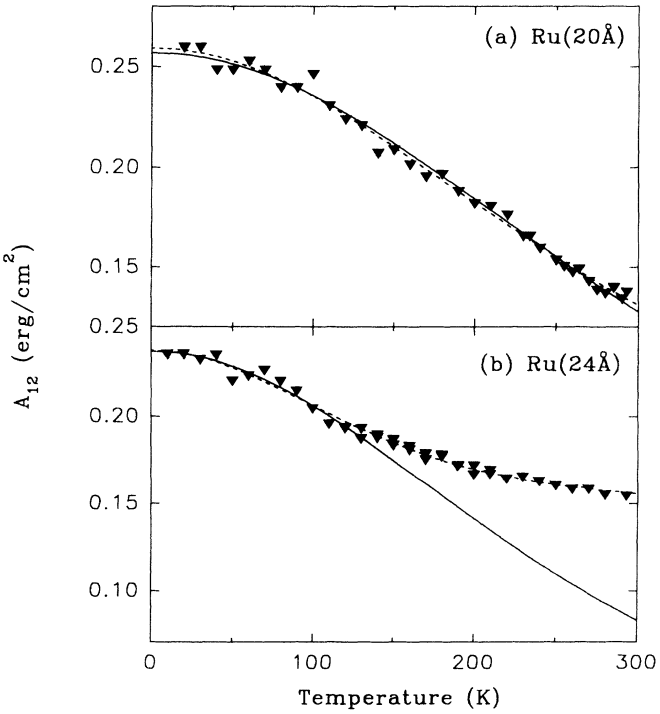

FIG. 18. Same as in Fig. 16 for (a) the Co(32 Å)/Ru(20 Å)/Co(32 Å) and (b) Co(32 Å)/Ru(24 Å)/Co(32 Å) samples.

due to the softening of the interfacial magnetism at high temperatures and has not been fully understood.

A better fit to the experimental data can be achieved for all four samples if Eq. (12) is modified as

$$A_{12}=[A_{12}(0)-A_{12}(\infty)]\frac{T}{T_0}\Big/\sinh\left[\frac{T}{T_0}\right]+A_{12}(\infty)\ , \tag{13}$$

where $A_{12}(\infty)$ is the exchange coefficient at $T=\infty$. The results are shown by the dotted lines in Figs. 17 and 18. A positive $A_{12}(\infty)$ was obtained in each sample, however, there is a large error in $A_{12}(\infty)$ due to the lack of experimental data at T significantly higher than T_0.

The fitting results using Eqs. (12) and (13) are listed in Table III. In each case, it can be seen that the characteristic temperature T_0 decreases with increasing Ru layer thickness and the values agree with the prediction of T_0 on the order of 100 K from the Edwards model.

The similarity between the experimental data and the theoretical predictions indicates that the interlayer exchange coupling mediated by the Ru spacer is closely related to the spatial confinement of d holes in the Ru layer due to a spin splitting of the d band in the Co layers. Using a simple-cubic tight-binding band model and an analog of the de Hass–van Alphen effect, the characteristic temperature T_0 can be expressed as[26]

$$T_0=\hbar v_F/2\pi k_B L\ , \tag{14}$$

where v_F is the Fermi velocity and L is the spacer thickness. By choosing suitable v_F, the theoretical predictions of T_0 were also listed in Table III which agree reasonably well with the experimental evaluation. The Fermi velocity used here is on the order of 10^7 cm/s, about an order of magnitude smaller than the values for most nonmagnetic materials predicted by a free-electron-gas model.[28] This can be explained because in the free-electron-gas model, the Fermi velocity is proportional to the Fermi wave vector k_F, while in Eq. (14), v_F is related to $\pi/a-k_F$, where a is the atomic layer distance in Ru. This result suggests that $\pi/a-k_F$ is much smaller than k_F in Ru, a condition necessary for the explanation of the long oscillation period observed in the Co/Ru/Co trilayer structures.[26,27]

C. Variation of A_{12} with the second Co layer thickness

While many studies have been devoted to the dependence of the interlayer exchange coupling A_{12} on the nonmagnetic layer thickness, little effort has been related to the dependence on the ferromagnetic layer thickness. In most of the theoretical calculations, the magnetic layer is assumed either to have infinite layer thickness[26] or to couple the nonmagnetic layer through its surface layer.[29] Recently, Barnas[18] and Bruno[19] calculated the magnetic layer thickness dependence of the interlayer exchange coupling in symmetrical trilayer systems (i.e., in each sample, $t_1=t_2$). Using a spin-split free-electron model, they predicted that the coupling strength depends on the magnetic layer thickness as well in an oscillatory manner due to Fabry-Perot-like interferences of the electron Bloch waves in the ferromagnetic layers. Since it is usually difficult to observe the optic mode for a symmetrical trilayer system, the asymmetrical Co/Ru/Co trilayer series was used for the study. In each asymmetrical series, the thickness of the second Co layer is the only variable parameter.

The two Co layers are antiparallel coupled for the Co(32 Å)/Ru(10 Å)/Co(t_2) (series III) and Co(32 Å)/Ru(12 Å)/Co(t_2) (series IV) series. In the in-plane magnetization curves for these samples, two transition fields $H_{cri,1}$ and $H_{cri,2}$ exist which separate the antiparallel, canted, and saturated states. Each transition field, as discussed in Sec. II, relates to the exchange-coupling coefficient as well as the thickness ratio between the two Co layers and therefore, can be used to evaluate A_{12} for these two series. Due to the frequency gap existing in the dispersion relation for these films, the FMR data could not provide sufficient information for the evaluation of the exchange coupling.

In series V having the structure Co(32 Å)/Ru(16 Å)/Co(t_2), the hysteresis loop is identical to that of a noncoupled system and cannot be used to evaluate the interlayer exchange coupling. However, two resonance modes were observed in both the X-band and K-band spectra in this series. Therefore, the angular dependence of the resonance field was used for the evaluation of A_{12}.

The variation of A_{12} with the thickness of the second Co layer t_2, is shown in Fig. 19 for the three asymmetri-

TABLE III. Fitting parameters of the interlayer exchange coupling A_{12} as a function of temperature for the symmetrical Co(32 Å)/Ru(t_{Ru})/Co(32 Å) structures. These parameters are defined by Eq. (12) for Edwards model and Eq. (13) for modified Edwards model. T_0^{ex} is the characteristic temperature evaluated from the experimental data and T_0^{th} is the theoretical predication using Eq. (14) with the Fermi velocity $v_F=1.7\times10^7$ cm/s for the Edwards model and $v_F=1.1\times10^7$ cm/s for the modified Edwards model.

		Edwards model			Modified Edwards model			
Series	t_{Ru} (Å)	T_0^{expt} (±20 K)	T_0^{th} (K)	$A_{12}(0)$ (erg/cm^2)	T_0^{expt} (±20 K)	T_0^{th} (K)	$A_{12}(0)$ (erg/cm^2)	$A_{12}(\infty)$ (erg/cm^2)
II	9	210	238	2.61	145	152	2.65	1.12
I	9.5	225	218	1.33	145	139	1.34	0.65
I	20	135	105	0.26	115	67	0.26	0.05
I	24	108[a]	87	0.24	60	56	0.24	0.15

[a]Obtained from the data at low temperatures.

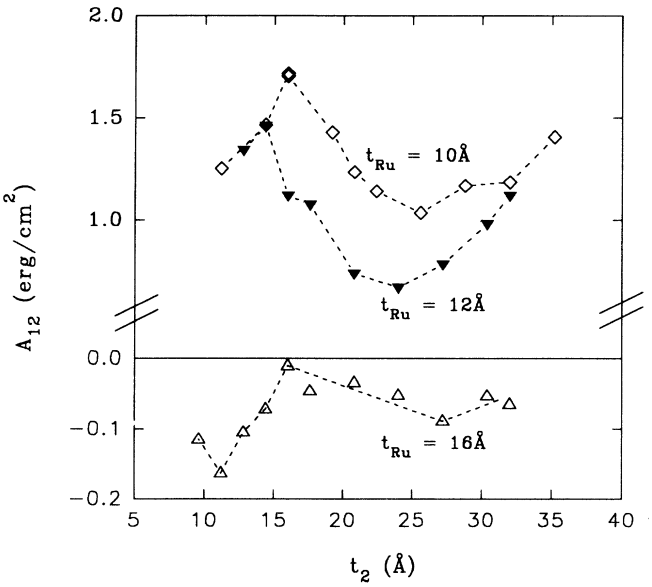

FIG. 19. The evaluation of A_{12} as a function of the second Co layer thickness t_2 for the three asymmetrical series (III, IV, and V) having the structure of Co(32 Å)/Ru(t_{Ru})/Co(t_2) with $t_{Ru}=10$, 12, and 16 Å, respectively. All results are at room temperature.

cal structures. The sign of A_{12} does not change within each series but the amplitude of A_{12} varies rather significantly as a function of t_2. In the two antiparallel coupled series and with increasing the second Co layer thickness, $|A_{12}|$ increases for $t_2 \leq 16$ Å, decreases for $16 \leq t_2 \leq 25$ Å and increases again for $25 \leq t_2 \leq 35$ Å. The variation amplitude, $|A_{12}^{\max}| - |A_{12}^{\min}|$, is about half of the average value of $|A_{12}|$ for each series which is larger than the theoretical predictions for the case of symmetrical structures.[19] In the parallel coupled series (series V), $|A_{12}|$ also reaches extreme values at $t_2 \sim 15$ and 25 Å. However, there is a 180° phase difference in comparison with the two antiparallel coupled series. $|A_{12}|$ in this series is a minimum (about 0.01 erg/cm^2) at $t_2 \sim 15$ Å but a maximum (about 0.17 erg/cm^2) at $t_2 \sim 25$ Å. This is also opposed to the predictions in the symmetrical structures.[19]

These results indicate that there is a variation of A_{12} with the magnetic layer thickness, which might be due to different Fabry-Perot-like interferences of the electron Bloch waves within the individual magnetic layers. The variation length Δt_2 is much larger than the π/k_F predicted from the free-electron model, suggesting that the discreteness of the magnetic layer thickness and of the moment distribution may have to be taken into account.[27]

D. Effective uniaxial anisotropy field $H_{u2,i}^{\text{eff}}$

The effective anisotropy field $H_{u2,i}^{\text{eff}}$ depends sensitively on the thickness of the Co layer and the temperature as well as the growth quality. In the first series of samples, there generally exists a 1–3 kG difference in H_{u2}^{eff} between the first and the second Co layers which originates from the large number of stacking defaults observed in the second Co layer. This difference in H_{u2}^{eff} is greatly reduced in the second series as the growth quality of the film is improved.

In the asymmetrical structures, $H_{u2,2}^{\text{eff}}$ increases significantly with decreasing the second Co layer thickness t_2 while $H_{u2,1}^{\text{eff}}$ remains constant as shown in Fig. 20(a). The variation of $h_{u2,2}^{\text{eff}}$ with t_2 can be expressed using a bulk contribution $H_{\text{bulk}}^{\text{eff}}$ and a surface contribution H_s from each Co/Ru interface:

$$t_2 \cdot H_{u2,2}^{\text{eff}} = t_2 \cdot H_{\text{bulk}}^{\text{eff}} + 2H_s \ . \tag{15}$$

$H_{\text{bulk}}^{\text{eff}}$ is about -12.2 kG in these samples which agrees with the estimation using the demagnetization field (-17.6 kG) and the uniaxial anisotropy field (5.9 kG) of bulk Co. The surface anisotropy field H_s is quite large in these samples and corresponds to a surface anisotropy energy of $K_s \sim 0.40$ erg/cm^2. The origin of this surface anisotropy energy might come from the magnetoelastic anisotropy energy due to the lattice expansion of the Co near the Co/Ru interfaces.[20] From Eq. (14), the Co layer will have a perpendicular uniaxial anisotropy (i.e., $H_{u2}^{\text{eff}} > 0$) when its thickness is less than 10 Å. This is confirmed by the FMR measurements and the magnetization measurements performed on ultrathin Co layer films

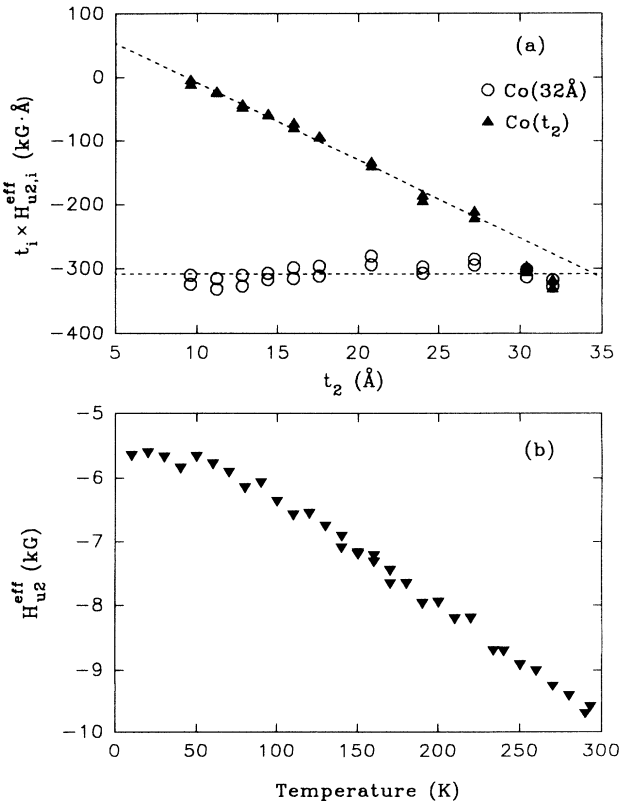

FIG. 20. (a) The evaluation of $t_i H_{u2,i}^{\text{eff}}$ as a function of the second Co layer thickness t_2 for the Co(32 Å)/Ru(16 Å)/Co(t_2) series at room temperature. The dashed lines are best fit using the conditions described in the text. (b) Temperature dependence of H_{u2}^{eff} for the Co(32 Å)/Ru(9.5 Å)/Co(32 Å) sample.

with the external field applied both parallel and perpendicular to the film plane.

With decreasing temperature, $|H_{u2,i}^{\text{eff}}|$ decreases, suggesting an increase of the perpendicular uniaxial anisotropy field at low temperature. A typical variation of H_{u2}^{eff} with temperature is shown in Fig. 20(b).

V. CONCLUSION

The angular dependence of the exchange-coupled ferromagnetic resonance theory for a three-layer structure was presented in this paper. In comparison with the in-plane magnetization measurement, the resonance method can evaluate both the sign and the amplitude of the exchange interaction between the two ferromagnetic layers through the "nonmagnetic" spacer. Since FMR measures the dynamic properties of the system and are not sensitive to the domain structures of the film, the results are more reliable than those from the magnetization measurements.

The dispersion relation in each film depends on the exchange-coupling field as well as the internal anisotropy fields within each layer. Because there are several unknown parameters in the model, it is usually not possible to determine all of them from just the in-plane FMR spectra. In this case, the perpendicular FMR spectra as well as the spectra at arbitrary angles are found to be essential to evaluate those parameters.

Special attention has been focused on the unsaturated states of an antiparallel coupled system in which the dispersion relation is significantly modified from that of a noncoupled system. A frequency gap exists in the dispersion relation when the magnetic moment is not saturated, resulting the absence of the acousticlike resonance mode at low frequencies when the external field is applied close to the normal orientation. The optic mode, which has little or no microwave absorption in the standard FMR experiment, can be observed when the rf pumping is parallel to the bias field. These unique features provide extra information about the exchange-coupling strength and the uniaxial anisotropy energies and can be used to accurately determine those internal parameters and their variation with the change of external conditions.

The exchange-coupled resonance theory has been applied to investigate the interlayer exchange coupling in the Co/Ru/Co trilayer structures and its variation with the Ru layer thickness, the Co layer thickness, and temperature. The results revealed the following.

(i) Only the bilinear exchange coupling term has been observed in these samples. The biquadratic coupling term is at least 2 orders of magnitude smaller than the bilinear term.

(ii) For extremely thin Ru layer thickness, the Co layers are strongly antiparallel coupled. This agrees with the prediction from the band-structure calculation.

(iii) Both the sign and the amplitude of A_{12} oscillate with the increase of the Ru layer thickness. The oscillation period is about 10 Å. No short period oscillations were observed.

(iv) The oscillation period and phase do not change upon decreasing the temperature. However, the oscillation amplitude is significantly enhanced at low temperatures. The variation of A_{12} with temperature follows roughly the relationship predicted by the theoretical models (Refs. 26 and 27). The characteristic temperature T_0 decreases with increasing the Ru spacer thickness.

(v) The exchange-coupling strength is also observed to depend on the magnetic layer thickness. With the change of the second Co layer thickness in the asymmetrical Co/Ru/Co structures, the variation amplitude ΔA_{12} is on the same order of A_{12} and the variation period is about 10 Å between the maximum and minimum values of A_{12}. No change in the sign of A_{12} has been observed in any of the series.

(vi) The effective uniaxial anisotropy field depends on the Co layer thickness as well as temperature.

ACKNOWLEDGMENTS

The authors would like to thank Dr. R. Stamps for fruitful discussions, Dr. G. Pan for providing the cross-sectional TEM image, and J. Arabski for preparing the samples. They would also like to acknowledge travel support from the North Atlantic Treaty Organization through Grant No. RG.930480.

[1]M. N. Baibich, J. M. Broto, A. Fert, F. Nguyen Van Dau, F. Petroff, P. Eitenne, G. Creuzet, A. Friederich, and J. Chazelas, Phys. Rev. Lett. **61**, 2472 (1988).

[2]P. Grunberg, R. Schreiber, and Y. Pang, Phys. Rev. Lett. **57**, 2442 (1986).

[3]M. Vohl, J. Barnas, and P. Grunberg, Phys. Rev. B **39**, 12 003 (1989).

[4]B. Heinrich, S. T. Purcell, J. R. Dutcher, K. B. Urquhart, J. F. Cochran, and A. S. Arrott, Phys. Rev. B **38**, 12 879 (1988).

[5]B. Hillebrands, Phys. Rev. B **37**, 9885 (1988).

[6]J. J. Krebs, P. Lubitz, A. Chaiken, and G. A. Prinz, Phys. Rev. Lett. **63**, 1645 (1989); J. J. Krebs, P. Lubitz, A. Chaiken, and G. A. Prinz, J. Appl. Phys. **67**, 5920 (1990).

[7]Z. Zhang, P. E. Wigen, and K. Ounadjela, IEEE Trans. Magn. **29**, 2717 (1993).

[8]J. F. Cochran, J. Rudd, W. B. Muir, B. Heinrich, and Z. Celinski, Phys. Rev. B **42**, 508 (1990).

[9]P. E. Wigen, Z. Zhang, L. Zhou, M. Ye, and J. A. Cowen, J. Appl. Phys. **73**, 6338 (1993).

[10]S. S. P. Parkin, N. More, and K. P. Roche, Phys. Rev. Lett. **64**, 2304 (1990).

[11]J. F. Cochran, B. Heinrich, and A. S. Arrott, Phys. Rev. B **34**, 7788 (1988).

[12]For a review see, e.g., P. Grunberg, Prog. Surf. Sci. **18**, 1 (1985).

[13]Dr. A. Slavan (private communication).

[14]M. Ruhrig, R. Schafer, A. Hubert, R. Mosler, J. A. Wolf, S. Demokritov, and P. Grunberg, Phys. Status. Solid A **125**, 635 (1991).

[15]M. E. Filipkowski, C. J. Gutierrez, J. J. Krebs, and G. A. Prinz, J. Appl. Phys. **73**, 5963 (1993).

[16]A. Layadi and J. O. Artman, J. Magn. Magn. Mater. **92**, 143 (1990).

[17]P. E. Wigen and Z. Zhang, Braz. J. Phys. **22**, 267 (1992).

[18]J. Barnas, J. Magn. Magn. Mater. **111**, L125 (1992).
[19]P. Bruno, Europhys. Lett. **23**, 615 (1993).
[20]D. Muller, K. Ounadjela, P. Vennegues, V. Pierron-Bohnes, A. Arbaoui, J. P. Jay, A. Dinia, and P. Panissod, J. Magn. Magn. Mater. **104**, 1873 (1992).
[21]G. Pan, A. Michel, V. Pierron, P. Vennegus, and M. C. Cadeville (unpublished).
[22]D. Stoeffler, K. Ounadjela, and F. Cautier, J. Magn. Magn. Mater. **93**, 386 (1991).
[23]C. Meny and P. Panissod (private communication).
[24]A. Dinia and K. Ounadjela (unpublished).
[25]A. M. Clogston, H. Suhl, L. R. Walker, and P. W. Anderson, J. Phys. Chem. Solids **1**, 129 (1956).
[26]D. M. Edwards, J. Mathon, R. B. Muniz, and M. S. Phan, Phys. Rev. Lett. **67**, 493 (1991).
[27]P. Bruno and C. Chappert, Phys. Rev. Lett. **67**, 1602 (1992); P. Bruno and C. Chappert, Phys. Rev. B **46**, 261 (1992).
[28]For example, see N. W. Ashcroft and N. D. Mermin, *Solid State Physics* (Saunders College HRW, Philadelphia, 1976).
[29]Y. Wang, P. M. Levy, and J. L. Fry, Phys. Rev. Lett. **65**, 2732 (1990).

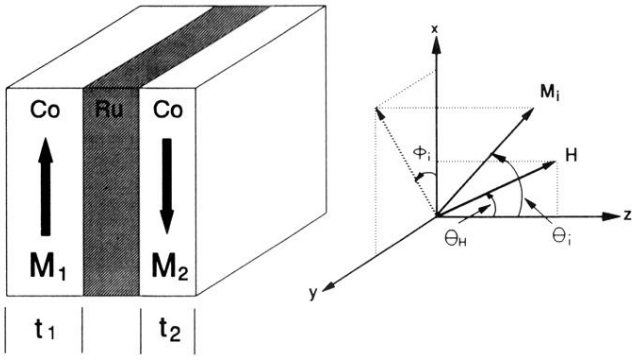

FIG. 1. The trilayer structure and coordinate system used in the model.

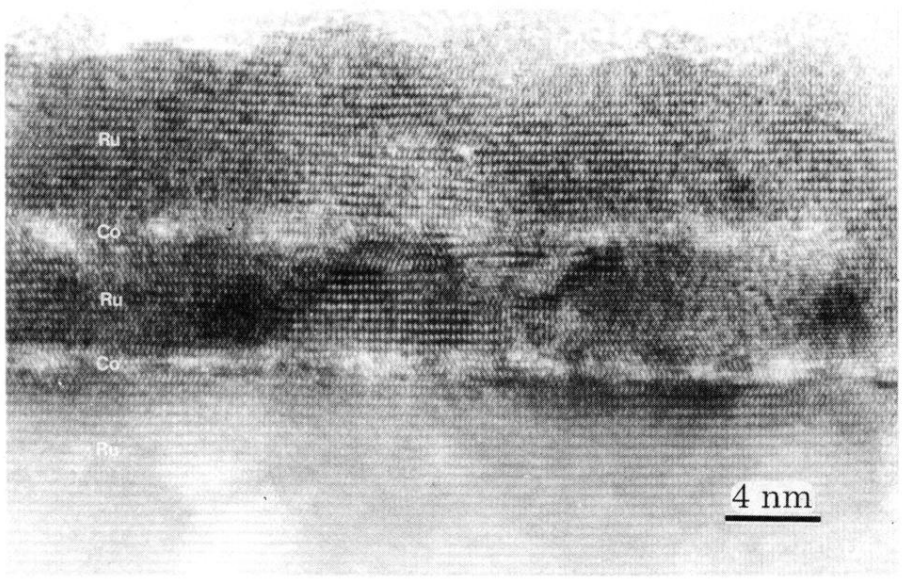

FIG. 9. Cross-sectional high-resolution TEM image of the Co(12 Å)/Ru(35 Å)/Co(12 Å) trilayer structure [from G. Pan (Ref. 21)].